

Inclusive versus Exclusive EM Processes  
in Relativistic Nuclear Systems <sup>1]</sup>This work is  
supported in part by funds provided by the  
U.S. Department of Energy (D.O.E.) under  
cooperative agreement  
#DE-FC01-94ER40818.

MIT/CTP #2523 <sup>2]</sup>Submitted to *Phys. Rev.*  
<sup>C</sup> <sup>3]</sup>PACS 25.30

R.Cenni<sup>†</sup>, T.W.Donnelly<sup>‡</sup> and A.Molinari<sup>‡</sup>

<sup>†</sup>Dipartimento di Fisica – Università di Genova  
Istituto Nazionale di Fisica Nucleare – sez. di Genova  
Via Dodecaneso, 33 – 16146 Genova (Italy)

<sup>‡</sup> Center for Theoretical Physics  
Laboratory for Nuclear Science and Department of Physics  
Massachusetts Institute of Technology  
Cambridge, Massachusetts 02139, U. S. A.

<sup>‡</sup> Dipartimento di Fisica Teorica dell’Università di Torino  
Istituto Nazionale di Fisica Nucleare – Sez. di Torino  
Via P. Giuria, 1 – 10125 Torino (Italy)

14 June 1996

---

\*[  
†[  
‡[

## Abstract

**Abstract:** Connections are explored between exclusive and inclusive electron scattering within the framework of the relativistic plane-wave impulse approximation, beginning with an analysis of the model-independent kinematical constraints to be found in the missing energy–missing momentum plane. From the interplay between these constraints and the spectral function basic features of the exclusive and inclusive nuclear responses are seen to arise. In particular, the responses of the relativistic Fermi gas and of a specific hybrid model with confined nucleons in the initial state are compared in this work. As expected, the exclusive responses are significantly different in the two models, whereas the inclusive ones are rather similar. By extending previous work on the relativistic Fermi gas, a reduced response is introduced for the hybrid model such that it fulfills the Coulomb and the higher-power energy-weighted sum rules. While incorporating specific classes of off-shellness for the struck nucleons, it is found that the reducing factor required is largely model-independent and, as such, yields a reduced response that is useful for extracting the Coulomb sum rule from experimental data. Finally, guided by the difference between the energy-weighted sum rules of the two models, a version of the relativistic Fermi gas is devised which has the 0<sup>th</sup>, 1<sup>st</sup> and 2<sup>nd</sup> moments of the charge response which agree rather well with those of the hybrid model: this version thus incorporates *a priori* the binding and confinement effects of the struck nucleons while retaining the simplicity of the original Fermi gas.

# 1 Introduction

The relativistic non-interacting Fermi gas (RFG) is a rare example of a three-dimensional many-body system that can be solved while fully respecting Lorentz covariance. When used in interpreting inclusive electron scattering at energies and momentum transfers that are not too small (*i.e.*, at the scales set by the Fermi momentum) it leads to results that qualitatively account for the existing data. It thus seems natural to ask the question: for exclusive processes, *e.g.* for the coincidence experiment  $(e, e'p)$ , is the RFG able to account for experiment as well? The answer to this question is clearly negative.

One might then argue that the spectral function of the RFG, the key ingredient in obtaining the exclusive cross section in the framework of the Plane-Wave Impulse Approximation (PWIA), is severely out of touch with the physical world. Yet when integrated over the energies and directions of the outgoing nucleons it leads to sensible results. In other words the RFG provides an acceptable first approximation to the particle-hole Green's function, which is closely related to the inclusive cross section, but not to the single-particle propagator, which is closely related to the spectral function.

Of course, some of the failure of the RFG to explain such exclusive processes also, but clearly not only, arises from shortcomings shared with the PWIA in dealing with the  $(e, e'p)$  reaction through neglect of final-state interactions. In this work we limit our focus to kinematics where such effects are believed to be small and accordingly where the PWIA should provide a good starting point.

With this as background, let us now state the motivations for the present work: we explore within the framework of the PWIA the connection between

exclusive and inclusive EM processes with the aim of

1. deepening the understanding of the RFG model;
2. assessing the impact of confinement effects for struck nucleons in a finite nucleus on the inclusive charge response function by exploring a specific hybrid model (to be defined in detail later) whose simple, tractable form facilitates taking the limit  $A \rightarrow \infty$ ;
3. providing a link between finite and infinite Fermi systems in searching for a common *model-independent* factor to be used in defining a reduced charge response such as to have the Coulomb sum rule fulfilled and
4. exploring whether a modified RFG charge response can be worked out in such a way that, on the average, incorporates some of the properties of a confined system described in a mean-field framework.

To start with in sec. 2 and 3 the kinematics of exclusive processes and the PWIA are shortly revisited together with the definitions and basic properties of the scaling variable and spectral function. In sec. 4 the inclusive cross sections and associated nuclear responses are obtained by suitably integrating over the exclusive processes. In particular we pay attention to the problem of fixing a dividing factor to yield a reduced longitudinal response for a finite system such that it obeys the Coulomb sum rule.

Next, in sec. 5, we examine in some depth the RFG, including the associated spectral function and its support in the plane of the momentum and excitation energy of the daughter nucleus (often referred to as “missing momentum” and “missing energy”, respectively). In particular, by integrating the exclusive process over the variables of the outgoing nucleon, we recover

the well-known expression for the inclusive cross section of the RFG. This we achieve for  $q \geq 2k_F$  ( $q$  being the three-momentum transfer and  $k_F$  the Fermi momentum), but not for  $q < 2k_F$  where Pauli correlations play a role. Indeed the PWIA ignores all correlations between the outgoing nucleon and the daughter nucleus, including those stemming from the fermion statistics.

In sec. 6 we improve upon the spectral function of the RFG allowing the hole states to be bound by a harmonic oscillator potential, the particle states still being plane waves. Thus we set up a simple, tractable hybrid model (HM) to guide us in exploring the connections between finite and infinite Fermi systems. Our goal here is not to undertake computations with the best mean-field wave functions (which of course could be done using the ideas presented in this work), but to develop a model for the initial nuclear state where the nucleons are confined, on the one hand, and yet simply described, on the other. For such a model much of the analysis can be done analytically and it is feasible to consider very heavy nuclei: in sec. 6 we present results for closed major shell  $N = Z$  nuclei up to the (hypothetical) case  $A = 336$ . The harmonic oscillator HM represents an extreme when compared with the RFG in that the former has very strongly confined bound-state wave functions (with gaussian tails rather than exponentials as would be the case when finite potentials are used), whereas the latter only involves plane waves.

In inter-comparing the two models we find that the Fermi momentum  $k_F$  of the RFG cannot be adjusted to yield the correct root-mean-square momentum for each shell of a harmonic oscillator well of a given frequency  $\omega_0$ . To achieve this a set of RFG, each with its own  $k_F$ , is needed. When dealing with inclusive processes, however, one global  $k_F$  is usually selected to get the same response width as that produced in some other model such

as the HM. These alternatives are also discussed in sec. 6.

In the same section we continue with an assessment of the impact on the longitudinal response of the finite size of the bound nuclear system in a mean field–PWIA framework. We find that the positive separation energy (but not the confinement) of the nucleus induces a hardening of the longitudinal response with respect to the RFG result. On the basis of scaling arguments we quantify this energy shift through a simple, but useful expression for the difference between the HM and RFG energy-weighted sum rules. We search for a Fermi momentum  $k_F$  and for a shift of the excitation energy such as to account for the confinement and separation energy of the nucleons in the initial state when calculating the longitudinal response within the framework of the RFG model. We accomplish this by comparing the inclusive charge response of the HM and of the RFG together with their various moments (the sum rule, mean excitation energy and variance).

We succeed as well in solving the problem of finding a reduction factor for the charge response in a way that permits the single-nucleon physics to be factored out and the Coulomb sum rule to be satisfied asymptotically. In this connection we extend a result found previously for the RFG. Namely, the reduction factor devised for the RFG is valid as well for the HM with harmonic oscillator wave functions and, by extension, suggests that such a definition should prove to be useful for wide classes of mean-field potentials.

Finally, our conclusions are presented in sec. 7.

## 2 The kinematics

In this section we consider exclusive (semi-inclusive) nuclear electron scattering where the final electron is detected in coincidence with an outgoing

nucleon, as described by the diagram of fig. 1 in the one-photon-exchange approximation. The associated cross section (in the laboratory system where the target four-momentum is  $P^\mu = (M_A^0, 0)$ , with  $M_A^0$  the initial ground-state mass, and differential with respect to both the outgoing electron and nucleon variables) reads [1]

$$\frac{d^4\sigma}{d\varepsilon'd\Omega_e dE_N d\Omega_N} = \frac{4\alpha^2}{(2\pi)^3} \frac{m_e^2 M_{A-1} m_N p_N k'}{\varepsilon E_{A-1}} \times \frac{1}{Q^4} \eta_{\mu\nu} W^{\mu\nu} \delta(\omega + M_A^0 - E_N - E_{A-1}). \quad (1)$$

In the above the square of the (spacelike) four-momentum transfer is given by  $Q^2 = \omega^2 - q^2 < 0$ , where  $Q^\mu = (\omega, \mathbf{q})$ ,

$$\eta_{\mu\nu} = \frac{1}{2m_e^2} [K_\mu K'_\nu + K'_\mu K_\nu - g_{\mu\nu} K \cdot K'] \quad (2)$$

is the symmetric ultrarelativistic leptonic tensor and  $W^{\mu\nu}$  its hadronic counterpart whose expression will be discussed later. Furthermore,  $\mathbf{p}_N$  and  $E_N = (m_N^2 + p_N^2)^{1/2}$  are the momentum and energy of the ejected nucleon, *i.e.*,  $P_N^\mu = (E_N, \mathbf{p}_N)$ . The other variables are either self-explanatory or similar to those used in ref. [2] (recall also that  $e^2 = 4\pi\alpha$ ).

In deriving eq. (1) the conventions of Bjorken and Drell [3] have been used. As a consequence the single-nucleon states are normalized according to

$$\langle \mathbf{p} | \mathbf{q} \rangle = (2\pi)^3 \frac{E(\mathbf{p})}{m_N} \delta(\mathbf{p} - \mathbf{q}), \quad (3)$$

with  $E(\mathbf{p}) = (m_N^2 + p^2)^{1/2}$ , which is consistent with the anticommutation rule

$$\{\hat{a}_p^\dagger, \hat{a}_q\} = (2\pi)^3 \frac{E(\mathbf{p})}{m_N} \delta(\mathbf{p} - \mathbf{q}) \quad (4)$$

for the fermion operators. For the initial ( $|A\rangle$ ) and daughter ( $|A-1\rangle$ ) unfragmented nuclear states we use the normalization

$$\langle A|A\rangle = \frac{E_A^0}{M_A^0} = 1, \quad \langle A-1|A-1\rangle = \frac{E_{A-1}}{M_{A-1}} \quad (5)$$

(throughout we work in the laboratory system where the initial nucleus is at rest). Note that when the state  $|A-1\rangle$  is fragmented its normalization is given by the product of the normalizations of the fragments and in such a case eq. (1) should be modified accordingly.

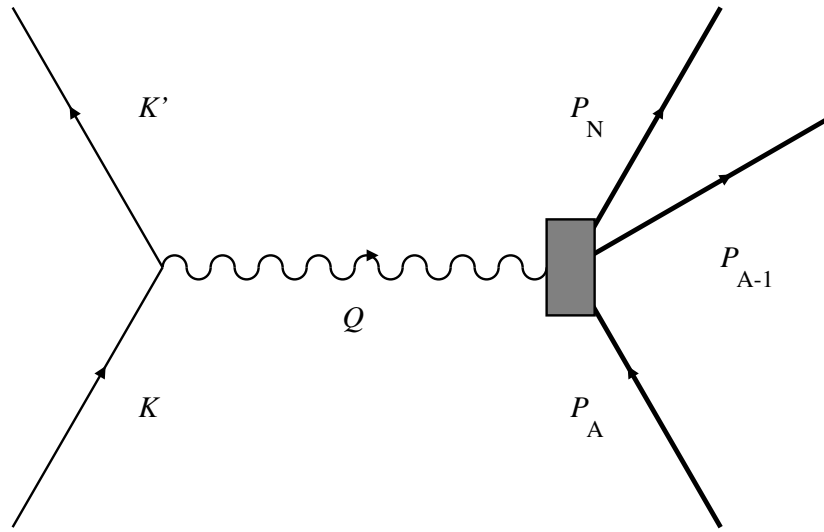


Figure 1: The diagram describing the coincidence process  $(e, e'p)$ .

Let us now discuss the energy-conserving  $\delta$ -function in eq. (1); for this purpose it helps to introduce, following ref. [4], the non-negative variable

$$\mathcal{E} = E_{A-1} - E_{A-1}^0 = \sqrt{\mathbf{p}_{A-1}^2 + (M_{A-1})^2} - \sqrt{\mathbf{p}_{A-1}^2 + (M_{A-1}^0)^2}, \quad (6)$$

which represents the excitation energy of the residual  $A-1$  nucleus moving with momentum  $\mathbf{p}_{A-1}$ . Here  $E_{A-1}$  is the energy of the daughter system when

it is generally excited, while  $E_{A-1}^0$  is the energy when in its ground state. In the laboratory frame, where  $\mathbf{p}_A = 0$ , one has necessarily that  $\mathbf{p}_{A-1} = -\mathbf{p}$ , if  $\mathbf{p}_N = \mathbf{p} + \mathbf{q}$  is the momentum of the outgoing nucleon. The argument of the  $\delta$ -function then vanishes for

$$\omega = \mathcal{E} + E_S + \left( \sqrt{(\mathbf{p} + \mathbf{q})^2 + m_N^2} - m_N \right) + \left( \sqrt{\mathbf{p}^2 + (M_{A-1}^0)^2} - M_{A-1}^0 \right), \quad (7)$$

where (for a stable nucleus) the non-negative separation energy

$$E_S = M_{A-1}^0 + m_N - M_A^0 \geq 0 \quad (8)$$

has been introduced.

Another energy that will prove to be relevant in our later discussions is  $E \equiv E_N - \omega$ , that is, we have  $P^\mu \equiv P_N^\mu - Q^\mu = (E, \mathbf{p})$ . In general  $P^2 = E^2 - p^2 \neq m_N^2$  and thus the kinematics for this four-vector are not those of an on-shell nucleon. Defining the daughter ground-state recoil kinetic energy  $T_{A-1}^0 \equiv E_{A-1}^0 - M_{A-1}^0$  we may use eq. (7) to write

$$E = m_N - (\mathcal{E} + E_S + T_{A-1}^0). \quad (9)$$

This may then be compared with the energy of an on-shell nucleon having three-momentum  $p$ , namely, using the nomenclature of ref. [5]

$$\bar{E} \equiv E(\mathbf{p}) = (p^2 + m_N^2)^{1/2} \quad (10)$$

yielding

$$\bar{E} - E = E_S + (\mathcal{E} + \bar{E} - m_N) + T_{A-1}^0. \quad (11)$$

In sec. 4, 5 and 6 we shall return to make use of eq. (11).

As discussed in ref. [4], it is then a simple matter to identify in the  $(\mathcal{E}, p)$  plane the domain that is compatible with the conservation of energy and

momentum for the process whose cross section is given by eq. (1). It turns out that

$$\mathcal{E}^+ \leq \mathcal{E} \leq \mathcal{E}^-, \quad (12)$$

where

$$\mathcal{E}^\pm = M_A^0 + \omega - \sqrt{p^2 + (M_{A-1}^0)^2} - \sqrt{(p \pm q)^2 + m_N^2} \quad (13)$$

and  $p = |\mathbf{p}|$ ,  $q = |\mathbf{q}|$ . Clearly the larger (smaller) excitation energy of the residual nucleus occurs when its momentum is parallel (antiparallel) to the momentum  $\mathbf{q}$  transferred to the system. Moreover  $\mathcal{E}^-$  is bounded according to

$$0 \leq \mathcal{E}^- \leq \omega - E_S - \left[ \sqrt{q^2 + (M_{A-1}^0 + m_N)^2} - (M_{A-1}^0 + m_N) \right], \quad (14)$$

since it reaches its maximum for a momentum

$$p = p_{\max} = q \frac{M_{A-1}^0}{M_{A-1}^0 + m_N}. \quad (15)$$

To provide an appreciation for the boundaries given by eq. (13) these are displayed in fig. 2 for  $q$  and  $\omega$  such that  $\mathcal{E}^\pm(0) < 0$ , namely for a point to the left of the quasielastic peak (QEP) of the inclusive response: the shaded domain in fig. 2 is where the semi-inclusive process can occur. On the other hand, for a point to the right of the RFG response peak, where  $\mathcal{E}^\pm(0) > 0$ , the allowed region is the one shown in fig. 3.

For use later we now briefly revisit the scaling variable, defined as [4]

$$y = -p_{\min}, \quad (16)$$

$p_{\min}$  being the smaller of the two real roots of the equation

$$\mathcal{E}^-(p) = 0. \quad (17)$$

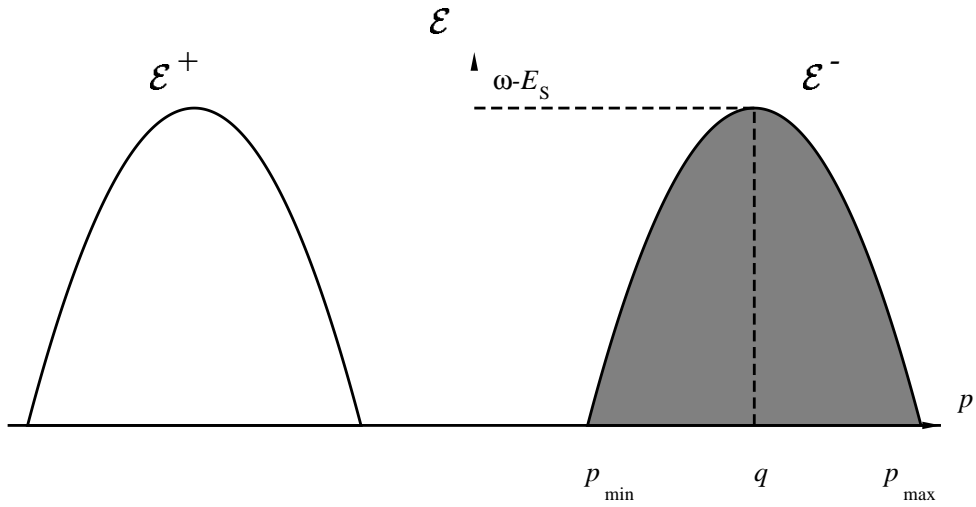


Figure 2: The curves  $\mathcal{E}^-$  and  $\mathcal{E}^+$  given by eq. (13) for a kinematics corresponding to the left side of the QEP. A semi-inclusive process can only occur within the shaded area.

Thus the scaling variable is (up to a sign) the smallest momentum at zero missing energy that a particle can have inside the nucleus in order to be active in a semi-inclusive process. The larger solution of eq. (17), customarily denoted by  $Y$ , will also be needed in the following. A direct calculation then yields

$$\begin{aligned}
 \left. \begin{aligned} y(q, \omega) \\ Y(q, \omega) \end{aligned} \right\} &= \frac{1}{2W^2} \\
 &\times \left\{ (M_A^0 + \omega) \sqrt{W^2 - (M_{A-1}^0 + m_N)^2} \sqrt{W^2 - (M_{A-1}^0 - m_N)^2} \right. \\
 &\quad \left. \mp q(W^2 + (M_{A-1}^0)^2 - m_N^2) \right\}, \tag{18}
 \end{aligned}$$

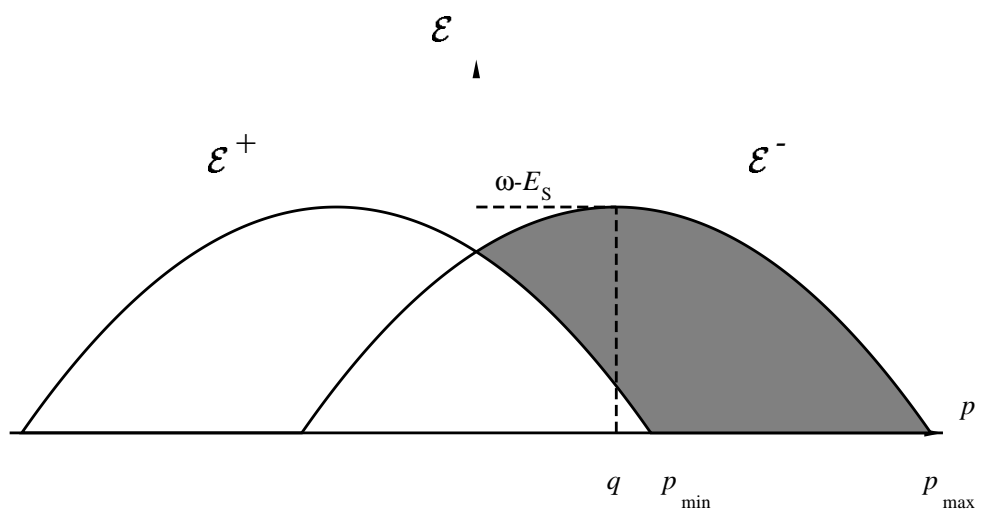


Figure 3: As in fig. 2, but for a kinematics corresponding to the right side of the QEP.

where  $W = \sqrt{(M_A^0 + \omega)^2 - q^2}$ . Notice that  $y$  and  $Y$  are defined in the range

$$\omega_t \leq \omega \leq q, \quad (19)$$

where

$$\omega_t = E_S + \sqrt{q^2 + (M_{A-1}^0 + m_N)^2} - (M_{A-1}^0 + m_N) \quad (20)$$

is the threshold energy. Also for

$$\omega = \omega_{\max} = E_S + \sqrt{q^2 + m_N^2} - m_N \quad (21)$$

the scaling variable vanishes.

In fig. 4 we display the monotonic behaviour of  $y$  versus  $\omega$  for fixed  $q$ . It reaches its minimum (negative) value  $y_{\min} = -p_{\max}$  (see eq. (15)) for  $\omega = \omega_t$ , while its maximum (positive) value is reached on the light front at  $y_{\max} = y(q, q)$ . Thus  $y_{\min}$  can be arbitrarily decreased by simply increasing  $q$ . In contrast,  $y_{\max}$  is bound by the limiting value

$$\lim_{q \rightarrow \infty} y_{\max}(q) = \frac{1}{2M_A^0} \left\{ (M_A^0)^2 - (M_{A-1}^0)^2 \right\} \sim m_N. \quad (22)$$

### 3 The impulse approximation

In this section we further elaborate the cross section given in eq. (1). This we do within the context of the PWIA which offers the simplest interpretation of the box of fig. 1 through the diagram displayed in fig. 5 in which the virtual photon is absorbed by a single nucleon inside the nucleus, the rest of the system acting as a spectator. We first consider the hadronic tensor

$$W^{\mu\nu} = \langle A | \hat{J}^\mu | F \rangle \langle F | \hat{J}^\nu | A \rangle, \quad (23)$$

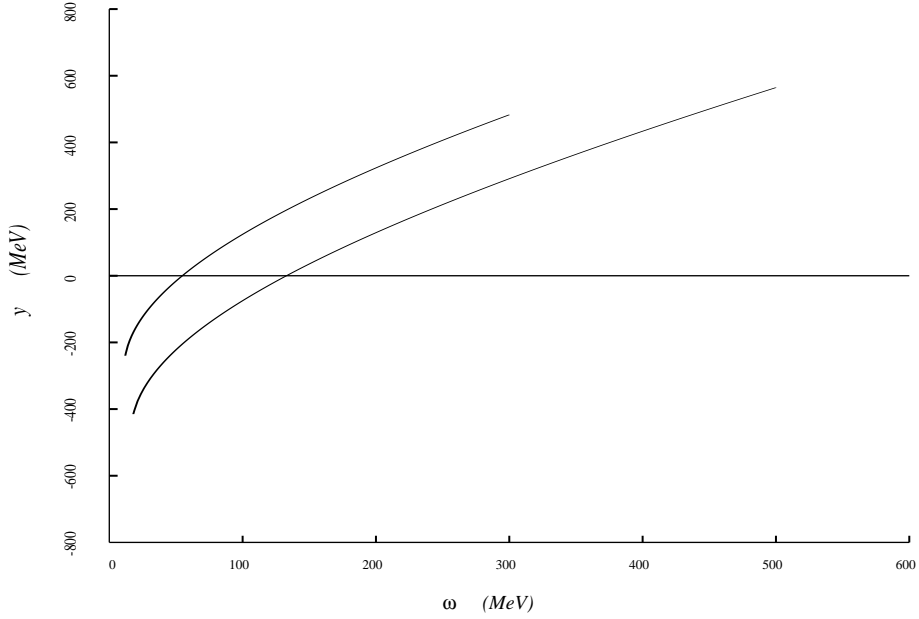


Figure 4: Frequency behaviour of the scaling variable for fixed  $|\mathbf{q}|$ . In the upper curve  $|\mathbf{q}| = 300$  MeV/c, while in the lower  $|\mathbf{q}| = 500$  MeV/c (in the figure  $A = 16$  and a separation energy of 8 MeV is assumed).

$|F\rangle$  being the continuum final state of the system system with  $A$  nucleons. In the impulse approximation only one-body hadronic currents are considered. These may be written

$$\hat{J}^\mu(Q) = \int \frac{d^3p}{(2\pi)^3} \int \frac{d^3p'}{(2\pi)^3} \frac{m_N}{E(\mathbf{p})} \frac{m_N}{E(\mathbf{p}')} \langle \mathbf{p}' | J^\mu(Q) | \mathbf{p} \rangle \hat{a}_{p'}^\dagger \hat{a}_p, \quad (24)$$

where

$$\langle \mathbf{p}' | J^\mu(Q) | \mathbf{p} \rangle = (2\pi)^3 \delta(\mathbf{p}' - \mathbf{p} - \mathbf{q}) (\mathbf{p} + \mathbf{q} | \Gamma^\mu(Q) | \mathbf{p}) \quad (25)$$

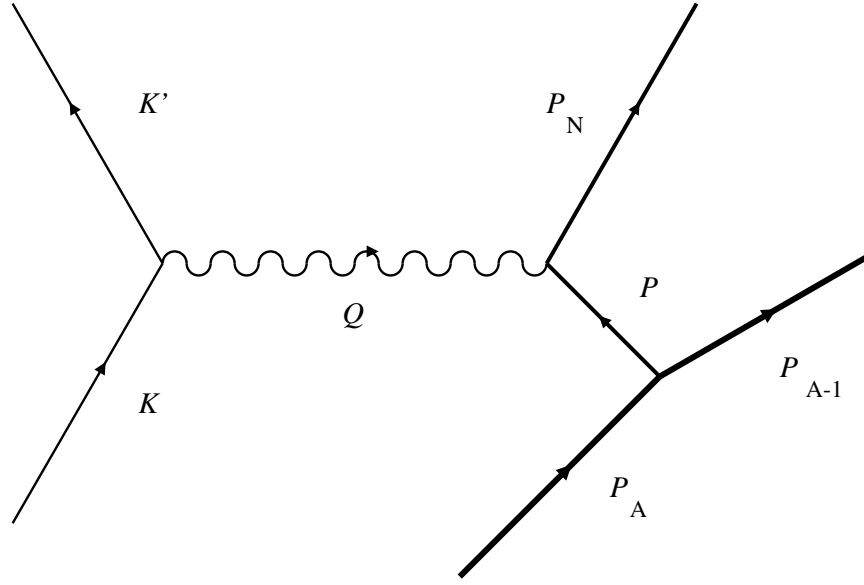


Figure 5: The PWIA interpretation of the box in fig. 1.

and  $\Gamma^\mu(Q)$  is the, in general off-shell, electromagnetic  $\gamma NN$  vertex operator.

On-shell one has

$$(\mathbf{p} + \mathbf{q}|\Gamma^\mu|\mathbf{p}) = \bar{u}(P + Q) \left[ \gamma^\mu F_1(Q^2) + \frac{i\sigma^{\mu\nu}}{2m_N} Q_\nu F_2(Q^2) \right] u(P), \quad (26)$$

as usual letting  $F_1$  and  $F_2$  be the Dirac and the Pauli form factors, whereas off-shell various prescriptions are commonly used [5] one of which is discussed in the next section.

The basic ingredient of the PWIA is embodied in the structure of the final state, which is factorized according to

$$\langle F | \hat{a}_{\mathbf{p}'}^\dagger = \langle \mathbf{p}_N | \mathbf{p}' \rangle \langle B | = (2\pi)^3 \frac{E(\mathbf{p}')}{m_N} \delta(\mathbf{p}_N - \mathbf{p}') \langle B |, \quad (27)$$

$|B\rangle$  being any of the excited states (including the ground state) that the residual  $A - 1$  nucleus might be left in (the factors in eq. (27) preserve

the normalization of  $\langle F \rangle$ . In eq. (27) the plane-wave description of the outgoing nucleon ignores its past history on its way out of the nucleus. We consider only kinematics where effects such as the distortion of the final-state nucleon wave function are expected to be small and thus, while our goal in the present work is focused on a model-to-model comparison, the results we obtain should be expected to be applicable at high  $q$  for roughly quasielastic kinematics. With the help of eqs. (24) and (27) the hadronic tensor is found to be

$$W^{\mu\nu} = \left( \frac{m_N}{E_{\mathbf{p}_N - \mathbf{q}}} \right)^2 \langle A | \hat{a}_{\mathbf{p}_N - \mathbf{q}}^\dagger | B \rangle \langle B | \hat{a}_{\mathbf{p}_N - \mathbf{q}} | A \rangle \mathcal{W}^{\mu\nu}(\mathbf{p}_N - \mathbf{q}, \mathbf{p}_N), \quad (28)$$

$$\mathcal{W}^{\mu\nu}(\mathbf{p}_N - \mathbf{q}, \mathbf{p}_N) = (\mathbf{p}_N - \mathbf{q} | \Gamma^{\dagger\mu} | \mathbf{p}_N) (\mathbf{p}_N | \Gamma^\nu | \mathbf{p}_N - \mathbf{q}) \quad (29)$$

being the single-nucleon tensor.

We can now recast the semi-inclusive cross section in the following form

$$\begin{aligned} \frac{d^4\sigma}{d\varepsilon' d\Omega_e dE_N d\Omega_N} &= \frac{4\alpha^2}{(2\pi)^3} \frac{m_e^2 m_N p_N k'}{\varepsilon} \frac{1}{Q^4} \left( \frac{m_N}{E(\mathbf{p}_N - \mathbf{q})} \right)^2 \\ &\times \eta^{\mu\nu} \mathcal{W}_{\mu\nu}(\mathbf{p}_N - \mathbf{q}, \mathbf{p}_N) \sum_{\beta} \frac{\langle A | \hat{a}_{\mathbf{p}_N - \mathbf{q}}^\dagger | A - 1, \beta \rangle \langle A - 1, \beta | \hat{a}_{\mathbf{p}_N - \mathbf{q}} | A \rangle}{\langle A - 1, \beta | A - 1, \beta \rangle} \\ &\times \delta(\omega + M_A^0 - E_N - E_{A-1}^\beta), \end{aligned} \quad (30)$$

where  $\beta$  runs over all possible quantum numbers of the  $A - 1$  nucleus, or, by exploiting completeness,

$$\begin{aligned} \frac{d^4\sigma}{d\varepsilon' d\Omega_e dE_N d\Omega_N} &= \frac{4\alpha^2}{(2\pi)^3} \frac{m_e^2 m_N p_N k'}{\varepsilon} \\ &\times \frac{1}{Q^4} \eta^{\mu\nu} \left( \frac{m_N}{E(\mathbf{p}_N - \mathbf{q})} \right)^2 \mathcal{W}_{\mu\nu}(\mathbf{p}_N - \mathbf{q}, \mathbf{p}_N) \\ &\times \langle A | \hat{a}_{\mathbf{p}_N - \mathbf{q}}^\dagger \delta(\omega + M_A^0 - E_N - E_{A-1}^0 - \hat{\mathcal{H}}) \hat{a}_{\mathbf{p}_N - \mathbf{q}} | A \rangle. \end{aligned} \quad (31)$$

In the above the Hamiltonian  $\hat{\mathcal{H}} = \hat{H} - E_{A-1}^0$ , acting on the quantum states of the  $A-1$  system, yields the excitation energies  $\mathcal{E}$ . Setting  $E = E_N - \omega$ , the energy of a nucleon inside the nucleus as above, and  $\mu = M_A^0 - E_{A-1}^0$ , the chemical potential we introduce the spectral function (our notation is chosen so as to maintain the standard definitions in the literature [6])

$$\tilde{S}(\mathbf{q}, q_0) = \frac{1}{(2\pi)^3} \frac{m_N}{E(\mathbf{q})} \frac{\langle A | \hat{a}_q^\dagger \delta[q_0 + \hat{\mathcal{H}} - \mu] \hat{a}_q | A \rangle}{\langle A | A \rangle}, \quad (32)$$

which obeys the model-independent relations

$$\sum_{\substack{\text{spin} \\ \text{isospin}}} \int_{-\infty}^{\infty} dE \tilde{S}(\mathbf{p}, E) = n(p) \quad (33)$$

and

$$\sum_{\substack{\text{spin} \\ \text{isospin}}} \int d^3p \int_{-\infty}^{\infty} dE \tilde{S}(\mathbf{p}, E) = A. \quad (34)$$

In eq. (33)  $n(p)$  is the momentum distribution of the nucleons in the nucleus.

Then it is an easy matter to re-express the cross section as

$$\frac{d^4\sigma}{d\varepsilon' d\Omega_e dE_N d\Omega_N} = E_N p_N \left( \frac{d\sigma}{d\Omega} \right)_{eN} \tilde{S}(\mathbf{p}, E), \quad (35)$$

where

$$\begin{aligned} \left( \frac{d\sigma}{d\Omega} \right)_{eN} &= \frac{4\alpha^2}{Q^4} m_e^2 \frac{k'}{\varepsilon} \frac{m_N^2}{E(\mathbf{p}) E_N} \eta^{\mu\nu} \mathcal{W}_{\mu\nu}(\mathbf{p}, \mathbf{p} + \mathbf{q}) \\ &= \sigma_M \frac{1}{\cos^2 \frac{\theta}{2}} \frac{m_e^2}{\varepsilon \varepsilon'} \eta^{\mu\nu} \frac{M_N^2}{E(\mathbf{p}) E_N} \mathcal{W}_{\mu\nu}(\mathbf{p}, \mathbf{p} + \mathbf{q}) \end{aligned} \quad (36)$$

is the cross section for elastic  $eN$  scattering and

$$\sigma_M = \frac{4\alpha^2}{Q^4} (\varepsilon')^2 \cos^2 \frac{\theta}{2} \quad (37)$$

is usual the Mott cross section. Projections of the single-nucleon tensor  $\mathcal{W}_{\mu\nu}$ , both on- and off-shell, are discussed in the next section.

## 4 The inclusive cross section, response functions and sum rule

To recover the inclusive cross section in the quasielastic region from eq. (35) an integration should be performed over the outgoing nucleon's variables  $E_N$  and  $\Omega_N$  and a sum should be made over protons and neutrons. In the PWIA, however, it is natural to perform the integration in the  $(\mathcal{E}, p)$  plane. Henceforth we shall write the arguments of the spectral function as  $(\mathbf{p}, \mathcal{E})$  rather than  $(\mathbf{p}, E)$  as in the last section. Clearly the variables are related by eq. (9). For the purpose of performing the integration we first add an integration over  $p$ , compensated by a  $\delta$ -function, to get

$$\frac{d^2\sigma}{d\Omega_e d\mathcal{E}'} = \int dE_N \int d^3p \left( \frac{d\sigma}{d\Omega} \right)_{eN} \tilde{S}(\mathbf{p}, \mathcal{E}) \delta \left( E_N - \sqrt{(\mathbf{p} + \mathbf{q})^2 + m_N^2} \right). \quad (38)$$

Next we introduce an azimuthal average over the single-nucleon cross section according to

$$\langle \sigma_0^{eN} \rangle = \frac{1}{2\pi} \int_0^{2\pi} d\phi \left( \frac{d\sigma}{d\Omega}(\mathbf{p}, \mathbf{q}) \right)_{eN}, \quad (39)$$

exploit the  $\delta$ -function to integrate over  $E_N$  and use the energy conservation to translate the remaining angular integration into one over  $\mathcal{E}$ . We thus obtain

$$\frac{d^2\sigma}{d\Omega_e d\mathcal{E}'} = \int_{\Sigma} dp d\mathcal{E} p^2 \frac{E_N}{pq} 2\pi \langle \sigma_0^{eN} \rangle \tilde{S}(\mathbf{p}, \mathcal{E}), \quad (40)$$

where  $\Sigma$  denotes the integration domain in the  $(\mathcal{E}, p)$  plane (shaded regions in figs. 2 and 3), or, more explicitly,

$$\int_{\Sigma} dp d\mathcal{E} \dots = \theta(-y) \int_{-y}^Y dp \int_0^{\mathcal{E}^-} d\mathcal{E} \dots + \theta(y) \left[ \int_0^y dp \int_{\mathcal{E}^+}^{\mathcal{E}^-} d\mathcal{E} \dots + \int_y^Y dp \int_0^{\mathcal{E}^-} d\mathcal{E} \dots \right]. \quad (41)$$

Let us now split the inclusive cross section into its longitudinal and transverse components setting

$$\frac{d^2\sigma}{d\Omega d\epsilon'} = \sigma_M \{v_L R_L(q, \omega) + v_T R_T(q, \omega)\}, \quad (42)$$

with

$$v_L = \left( \frac{Q^2}{q^2} \right)^2 \quad (43)$$

$$v_T = \frac{1}{2} \left| \frac{Q^2}{q^2} \right| + \tan^2 \frac{\theta}{2} \quad (44)$$

and, in terms of the components of the hadronic tensor in eq. (23),

$$R_L = W^{00} \quad (45)$$

$$R_T = W^{11} + W^{22}. \quad (46)$$

From eq. (40) it is then clear that the spectral function, which incorporates the nuclear dynamics, is channel independent and that the longitudinal or transverse nature of the response is reflected only in the single-nucleon cross section. After some algebraic manipulations of eq. (36) on-shell the latter can be cast in the form

$$\langle \sigma_0^{eN} \rangle = \sigma_M \frac{m_N}{E(\mathbf{p})} \frac{m_N}{E_N} [v_L \mathcal{R}_L + v_T \mathcal{R}_T], \quad (47)$$

with

$$\mathcal{R}_L = \frac{\kappa^2}{\tau} \left\{ \chi^2 [F_1^2(\tau) + \tau F_2^2(\tau)] + [F_1(\tau) - \tau F_2(\tau)]^2 \right\} \quad (48)$$

$$\mathcal{R}_T = \chi^2 [F_1^2(\tau) + \tau F_2^2(\tau)] + 2\tau [F_1(\tau) + F_2(\tau)]^2. \quad (49)$$

The factors in front of the right-hand side of eq. (47) are in accord with standard notation [2, 5]. Note also that the dimensionless variables  $\kappa =$

$q/2m_N$  and  $\tau = -Q^2/4m_N^2 = (q^2 - \omega^2)/4m_N^2$  have been introduced (in the following we shall also use the dimensionless transferred energy  $\lambda = \omega/2m_N$ ).

Moreover in the above

$$\chi \equiv \frac{p}{m_N} \sin \theta, \quad (50)$$

$\theta$  being the angle between  $\mathbf{p}$  and  $\mathbf{q}$ . For convenience we also quote an equivalent expression for the longitudinal single-nucleon response, *viz.*

$$\mathcal{R}_L = \frac{\kappa^2}{\tau} \left\{ G_E^2(\tau) + W_2(\tau) \chi^2 \right\}, \quad (51)$$

where

$$W_2(\tau) = \frac{1}{1 + \tau} \left[ G_E^2(\tau) + \tau G_M^2(\tau) \right] \quad (52)$$

is given in terms of the familiar Sachs nucleon form factors  $G_E$  and  $G_M$ .

All of the relations in eqs. (48, 49, 51) hold for a process with the initial nucleon in the vacuum and hence on-shell. Since the nucleon inside the nucleus is in general off-mass-shell, a prescription is required for its current. Here we follow the one labeled CC1 by De Forest [5] which sets

$$\overline{\omega} \equiv E_N - \overline{E} \quad (53)$$

$$\overline{\tau} \equiv \frac{q^2 - \overline{\omega}^2}{4m_N^2}, \quad (54)$$

where  $\overline{E}$  is given by eq. (10), and yields for the single nucleon's responses the expressions

$$\mathcal{R}_L = \frac{\kappa^2}{\overline{\tau}} \left\{ \chi^2 \left[ F_1^2(\tau) + \overline{\tau} F_2^2(\tau) \right] + [F_1(\tau) - \overline{\tau} F_2(\tau)]^2 \right\} \quad (55)$$

$$\mathcal{R}_T = \chi^2 \left[ F_1^2(\tau) + \overline{\tau} F_2^2(\tau) \right] + 2\overline{\tau} [F_1(\tau) + F_2(\tau)]^2, \quad (56)$$

*i.e.* in this off-shell prescription the energy transfer  $\omega$  is shifted in the single-nucleon responses, but not inside the form factors where it is kept unaltered.

The amount of the shift will be discussed further in sec. 6. We note in passing [2] that the CC2 prescription of De Forest [5] yields the same results as above for  $\mathcal{R}_L$  but not for  $\mathcal{R}_T$ . With the above definitions the nuclear responses finally read

$$R_{L,T}(q, \omega) = \int_{\Sigma} dp d\mathcal{E} p^2 \frac{E_N}{pq} 2\pi \tilde{S}(\mathbf{p}, \mathcal{E}) \frac{m_N}{\bar{E}} \frac{m_N}{E_N} \mathcal{R}_{L,T}(q, \bar{\omega}, p, \mathcal{E}). \quad (57)$$

Worth emphasizing here is the dependence of the single-nucleon responses upon  $\chi$ , in turn entailing a dependence upon the angle  $\theta$  and, through momentum conservation, upon  $p$  and  $\mathcal{E}$ . As a consequence, as already stressed in [7] and at variance with the non-relativistic case, the single-nucleon responses cannot be moved outside the integral over the  $\mathcal{E}$  and  $p$  variables, *i.e.*, they cannot be factorized.

With the responses fixed, a relativistic extension of the Coulomb sum rule and higher-order energy-weighted integrated responses can be obtained. In the non-relativistic case the Coulomb sum rule  $\Xi_0(q)$  is extracted from the data simply by dividing for  $G_E^2$  and one obtains for large  $q$  the well-known result  $\Xi_0(q) \rightarrow 1$ . In the relativistic case, where the integration over  $\omega$  is extended up to the light front and physical nucleons are considered, an appropriate reduction factor must be introduced in order to fulfill the sum rule.

Actually, as we shall discuss in detail in the following sections, a function  $H_L(q, \omega)$  can be defined such that

$$\frac{\mathcal{R}_L(q, \omega, p, \theta)}{H_L(q, \omega)} \sim 1 \quad (58)$$

in the whole domain where the spectral function is appreciably different from zero. As a consequence a Coulomb sum rule can be set up according to the

prescription (see below)

$$\Xi_0(q) = \int_{\omega_t}^q d\omega \int_{\Sigma} dp d\mathcal{E} \tilde{S}(p, \mathcal{E}) \frac{\mathcal{R}_L(q, \bar{\omega}, p, \theta)}{H_L(q, \bar{\omega})} \sim \int_{\omega_t}^q d\omega \int_{\Sigma} dp d\mathcal{E} \tilde{S}(p, \mathcal{E}), \quad (59)$$

with  $\omega_t$  given by eq. (20).

The difficulty in establishing the above relation stems from the fact that the integrals do not extend over the whole  $(\mathcal{E}, p)$  plane – in such a case one would invoke the sum rule for the spectral function, namely eq. (34), to validate the Coulomb sum rule at once. However, when  $q$  is sufficiently large, the integration domain actually encompasses the whole region of the  $(\mathcal{E}, p)$  plane where the nuclear spectral function is appreciably different from zero.

To illustrate this point we define the quantities

$$\mathcal{E}_{1,3} = M_A^0 + \omega_t - \sqrt{(M_{A-1}^0)^2 + p^2} - \sqrt{m_N^2 + (q \pm p)^2} \quad (60)$$

$$\mathcal{E}_{2,4} = M_A^0 + q - \sqrt{(M_{A-1}^0)^2 + p^2} - \sqrt{m_N^2 + (q \mp p)^2}, \quad (61)$$

which are nothing but the boundaries  $\mathcal{E}^{\pm}$  evaluated for the minimum allowed value of  $\omega$ , namely  $\omega_t$ , and for  $\omega$  on the light cone, respectively. Obviously no contribution to the integral in eq. (59) arises from the regions  $\mathcal{E} < \mathcal{E}_1$  and  $\mathcal{E} > \mathcal{E}_2$ . On the other hand, denoting the extreme values of  $\cos \theta$  by  $\cos \theta_{\min}$  and  $\cos \theta_{\max}$ , so that  $\cos \theta_{\min} \leq \cos \theta \leq \cos \theta_{\max}$ , then one can show that for  $\mathcal{E}_3 \leq \mathcal{E} \leq \mathcal{E}_4$  the integration range will have  $\cos \theta_{\min} = -1$  and  $\cos \theta_{\max} = +1$ . Under these circumstances the full sum rule can be attained; however, for  $\mathcal{E}_1 \leq \mathcal{E} < \mathcal{E}_3$  and  $\mathcal{E}_4 < \mathcal{E} \leq \mathcal{E}_2$  the full range of integration will not be available and one should expect the sum rule to be under-saturated. A final constraint is of course that  $\mathcal{E} \geq 0$ .

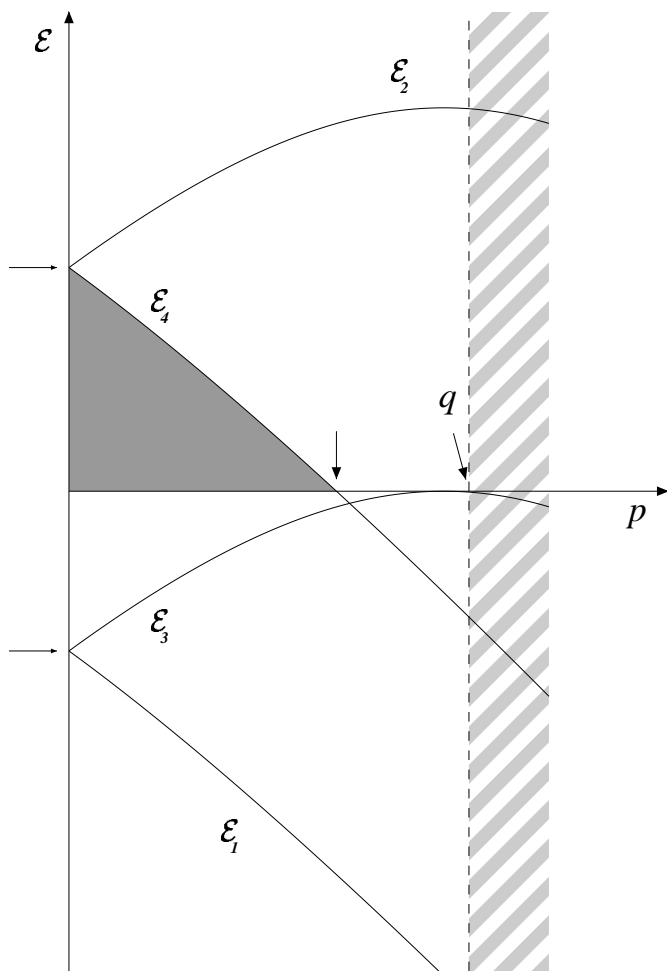


Figure 6: The boundaries of the integration region for the sum rule.

The typical behaviour of eqs. (60) and (61) is displayed in fig. 6. Several points on these curves are of particular significance and are indicated in the figure with arrows. Two include the  $\mathcal{E}$ -values at  $p = 0$ : in particular,

$$\mathcal{E}_2(0) = \mathcal{E}_4(0) = M_A^0 + q - M_{A-1}^0 - \sqrt{m_N^2 + q^2} \xrightarrow{q \rightarrow \infty} m_N - E_S, \quad (62)$$

which lies well above the scale of nuclear energies normally considered. Another is the value of  $p$  where  $\mathcal{E}_4(p) = 0$ , which occurs for

$$\begin{aligned} p &= \bar{p} = -\frac{q \left( (M_A^0)^2 + (M_{A-1}^0)^2 + 2M_A^0 q - m_N^2 \right)}{2M_A^0 (M_A^0 + 2q)} \\ &+ \frac{M_A^0 + q}{2M_A^0 (M_A^0 + 2q)} \sqrt{\left[ (M_A^0)^2 - (M_{A-1}^0)^2 - m_N^2 + 2M_A^0 q \right]^2 - 4(M_{A-1}^0)^2 m_N^2}. \end{aligned} \quad (63)$$

For large momentum transfers the above equation becomes

$$\bar{p} \xrightarrow{q \rightarrow \infty} \frac{(M_A^0)^2 - (M_{A-1}^0)^2}{2M_A^0} \sim m_N, \quad (64)$$

again well beyond the scale of momenta characterizing the nuclear momentum distribution.

In view of the magnitude of the above-quoted limiting values, it follows that for sufficiently large  $q$  the spectral function is expected to be concentrated in the shaded region of fig. 6. Thus, if a convenient form for the normalization factor  $H_L$  is found, then the sum rule over the spectral function automatically generates a sum rule over the longitudinal response. Within the context of the PWIA violation of the sum rule might then imply that significant contributions in the spectral function occur at very high missing energy and/or at very high missing momentum (both, of course, are absent in the models considered in the present work).

It is important to realize that the factor  $H_L$ , that accounts both for the kinematical factors of the single-nucleon cross section (solely due to relativity) and for the off-shellness of the single-nucleon response, turns out to be

largely model-independent. Its on-shell form will be given in the next section, while its off-shell extension will be discussed in sec. 6.

In concluding this section we also define the reduced longitudinal response

$$r_L(q, \omega) \equiv \frac{R_L(q, \omega)}{H_L(q, \omega)} \quad (65)$$

and the dimensionless energy-weighted moments according to

$$\Xi_n(q) = \int_0^q d\omega \lambda^n r_L(q, \omega), \quad (66)$$

where, as before,  $\lambda = \omega/2m_N$ . We shall examine some of these moments in the next two sections, together with the variance

$$\sigma(q) = \sqrt{\Xi_2(q) - (\Xi_1(q))^2}. \quad (67)$$

## 5 The Free Relativistic Fermi Gas

The free RFG should be considered as a paradigm for all fermion many-body systems. In its ground state the RFG has all its single-particle levels occupied by on-mass-shell nucleons up to the Fermi momentum  $k_F$ , a configuration with zero total momentum. Note that all states considered here in constructing this model are completely covariant, something that is usually given up in considering models with confinement, as in the next section. We write for the energy of the RFG initial state

$$M_A^{0,\text{RFG}} = 4 \sum_{k \leq k_F} \sqrt{\mathbf{k}^2 + m_N^2}. \quad (68)$$

Here  $A$  is a very large even integer to become infinite in the end and we consider only  $N = Z$  nuclei in the present work. If a particle is removed

from the surface of the RFG then the system thus obtained, which is clearly in its ground state (indicated by “0”), will have an energy

$$E_{A-1}^{0,\text{RFG}} = M_A^{0,\text{RFG}} - \sqrt{k_F^2 + m_N^2} \quad (69)$$

$$= \sqrt{(M_{A-1}^{0,\text{RFG}})^2 + k_F^2} \quad (70)$$

$$\equiv T_{A-1}^{0,\text{RFG}} + M_{A-1}^{0,\text{RFG}}. \quad (71)$$

It then follows that the daughter nucleus ground-state mass is given by

$$M_{A-1}^{0,\text{RFG}} = \sqrt{(M_A^{0,\text{RFG}})^2 - 2M_A^{0,\text{RFG}}\sqrt{k_F^2 + m_N^2} + m_N^2}. \quad (72)$$

Hence the separation energy of the RFG may be written

$$\begin{aligned} E_S^{\text{RFG}} &= M_{A-1}^{0,\text{RFG}} + m_N - M_A^{0,\text{RFG}} \\ &= \sqrt{(M_A^{0,\text{RFG}})^2 - 2M_A^{0,\text{RFG}}\sqrt{k_F^2 + m_N^2} + m_N^2} + m_N - M_A^{0,\text{RFG}} \\ &= -T_F - T_{A-1}^{0,\text{RFG}} \\ &\xrightarrow{A \rightarrow \infty} -T_F, \end{aligned} \quad (73)$$

where  $T_F \equiv (k_F^2 + m_N^2)^{1/2} - m_N \cong -k_F^2/2m_N$ . Note that  $E_S^{\text{RFG}}$  is negative, in contrast to the physical separation energy which must be positive.

We may also consider the  $(A - 1)$  Fermi gas in an excited state (namely with a hole inside the Fermi sphere) with an energy

$$\begin{aligned} \mathcal{E}^{\text{RFG}} &= [E_{A-1} - E_{A-1}^0]^{\text{RFG}} \\ &= \sqrt{k_F^2 + m_N^2} - \sqrt{p^2 + m_N^2}, \end{aligned} \quad (74)$$

which, since  $0 \leq p \leq k_F$ , is non-negative as it should be. Note also that this result together with eq. (11) imply that  $[\bar{E} - E]^{\text{RFG}} = 0$ , that is, as expected the struck nucleon is on-shell in the RFG model.

The curve obtained from eq. (74), and displayed in fig. 7 together with the region kinematically accessible to a semi-inclusive process for typical values of  $q$  and  $\omega$ , defines the support of the RFG spectral function  $\tilde{S}^{\text{RFG}}(\mathbf{p}, \mathcal{E})$ , *i.e.* the one-dimensional domain in the  $(\mathcal{E}, p)$  plane where it is non-vanishing.

As a consequence the RFG inclusive cross section is expected to reach its maximum, but for the influence of the single-nucleon physics, for  $\omega$  and  $q$  such that the domain of integration in the  $(\mathcal{E}, p)$  plane includes the whole of  $\tilde{S}^{\text{RFG}}(\mathbf{p}, \mathcal{E})$ . For this to occur it is required that at  $p=0$

$$\mathcal{E}^-(0) = \mathcal{E}^+(0) = \mathcal{E}^{\text{RFG}}(0), \quad (75)$$

which requires that

$$M_A^0 + \omega - M_{A-1}^0 - \sqrt{q^2 + m_N^2} = \sqrt{k_F^2 + m_N^2} - m_N. \quad (76)$$

Hence the well-known expression

$$\omega = \omega_{\text{QEP}} \equiv \sqrt{q^2 + m_N^2} - m_N = |Q^2|/2m_N \quad (77)$$

follows for the maximum of the RFG response.

To calculate  $\tilde{S}^{\text{RFG}}(\mathbf{p}, \mathcal{E})$  it helps to recall the Lehmann representation of the relativistic single-particle Green's function for an infinite, homogeneous system, which, disregarding antinucleonic components, reads

$$\begin{aligned} G_{\alpha\beta}(p, E(\mathbf{p})) &= \frac{1}{(2\pi)^3} \left( \frac{p' + m_N}{2Ep} \right)_{\alpha\beta} \frac{m_N}{E(\mathbf{p})} \\ &\times \left\{ < A | \hat{a}_{ps} \frac{1}{E(\mathbf{p}) - \hat{\mathcal{H}} - \mu + i\eta} \hat{a}_{ps}^\dagger | A > \right. \\ &\left. + < A | \hat{a}_{ps}^\dagger \frac{1}{E(\mathbf{p}) + \hat{\mathcal{H}} - \mu - i\eta} \hat{a}_{ps} | A > \right\}. \end{aligned} \quad (78)$$

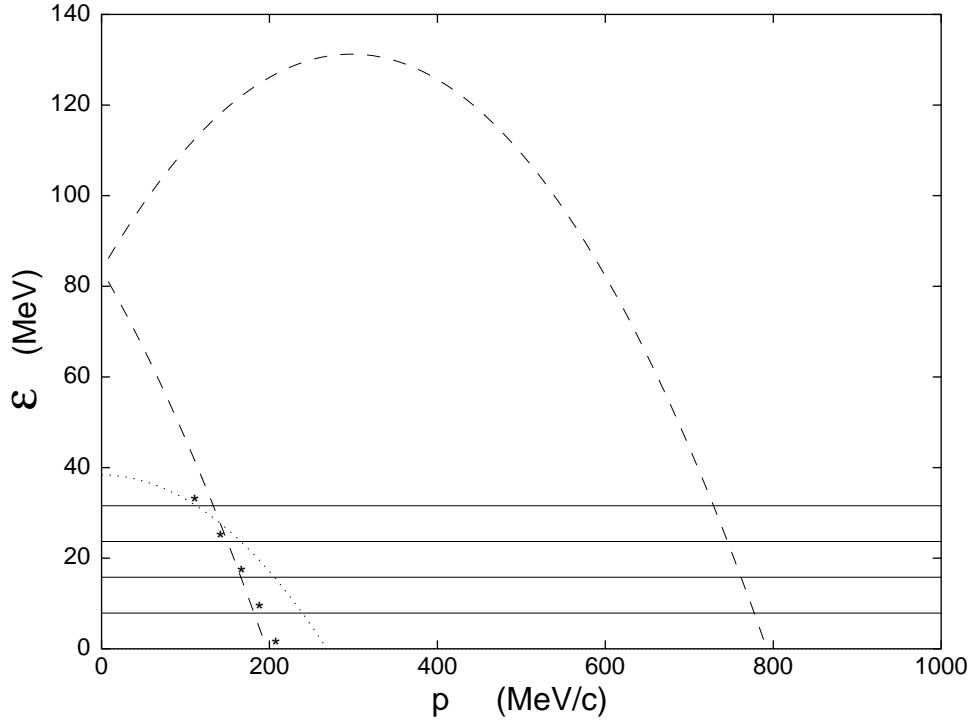


Figure 7: The support of the spectral function of a shell model nucleus with  $A = 140$  and  $N_{\max} = 4$  (parallel horizontal straight lines) with  $\omega_0 = 7.9$  MeV. Also shown is the support of the spectral function of the RFG as given by eq. (74) with  $k_F = 1.112 \text{ fm}^{-1}$  corresponding to the fictitious nucleus  $^{140}\text{Yb}$  (see eq. (119)). The stars correspond to the rms value of the momentum of a particle in a shell of given  $N$  (see eq. (118)). Finally the allowed domain for the exclusive process is shown for  $q = 300$  MeV and  $\omega = 100$  MeV (to the right of the response peak).

Then from eq. (32) the following connection between the hole part of the fermion propagator and the spectral function

$$\Im G_{\alpha\beta}^h(p) = \pi \left( \frac{p + m_N}{2E(\mathbf{p})} \right)_{\alpha\beta} \tilde{S}(\mathbf{p}, \mathcal{E}) \quad (79)$$

is found to hold true. For the RFG, whose states are normalized according to

$$\langle \mathbf{p} | \mathbf{q} \rangle = \Omega \frac{E(\mathbf{p})}{m_N} \delta_{p,q}, \quad (80)$$

$\Omega$  being the volume enclosing the system, rather than by eq. (3), one gets from eq. (79):

$$\begin{aligned} \tilde{S}^{\text{RFG}}(\mathbf{p}, \mathcal{E}) &= \frac{\Omega}{(2\pi)^3} \theta(k_F - p) \delta(E(\mathbf{p}) - \sqrt{p^2 + m_N^2}) \\ &= \frac{\Omega}{(2\pi)^3} \theta(k_F - p) \delta(\mathcal{E} - \sqrt{k_F^2 + m_N^2} + \sqrt{p^2 + m_N^2}), \end{aligned} \quad (81)$$

which is non-vanishing in the  $(\mathcal{E}, p)$  plane only along the curve defined by eq. (74).

To get the covariant RFG inclusive response we only need to insert eq. (81) into eq. (38), obtaining

$$\begin{aligned} \frac{d^2\sigma}{d\Omega_e d\mathcal{E}'} \Big|_{\text{RFG}} &= \Omega \int \frac{d^3p}{(2\pi)^3} \left( \frac{d\sigma}{d\Omega} \right)_{\text{eN}} \\ &\quad \theta(k_F - p) \delta \left( \omega - \left[ \sqrt{(\mathbf{p} + \mathbf{q})^2 + m_N^2} - \sqrt{p^2 + m_N^2} \right] \right), \end{aligned} \quad (82)$$

which is indeed recognized as the Pauli-unblocked RFG cross section. Note that the connection between exclusive and inclusive processes for the RFG can be established, in the PWIA framework, only in the Pauli unblocked region.

We now briefly consider the  $y$ -scaling properties of the RFG. In this model the onset of scaling is not induced by the behaviour of  $Y$ , which becomes

larger than any characteristic scale in the problem for large  $q$ , but by the spectral function, which fixes the upper integration limit over  $p$  to be  $k_F$ . Note furthermore that for the RFG the lower integration limit is not  $y$ , but rather the point where the support of the RFG spectral function intersects the boundary  $\mathcal{E}^\pm$ . Defining

$$y_{\text{RFG}} \equiv m_N \left[ \lambda \sqrt{1 + \frac{1}{\tau}} - \kappa \right], \quad (83)$$

we find that this intersection point occurs at  $p = |y_{\text{RFG}}|$ . The sign may be understood by making use of the  $\psi$ -scaling variable introduced in ref. [7]:

$$\psi = \frac{1}{\sqrt{\xi_F}} [2\theta(\lambda - \lambda_0) - 1] \left\{ \sqrt{(1 + \lambda)^2 + \frac{1}{\tau}(\tau - \lambda)^2} - (1 + \lambda) \right\}^{1/2}, \quad (84)$$

where

$$\xi_F = T_F/m_N = \sqrt{1 + \eta_F^2} - 1 \cong \eta_F^2/2 \quad (85)$$

since  $\eta_F \equiv k_F/m_N \cong 1/4$  is small. Here

$$\lambda_0 = \frac{\omega_{\text{QEP}}}{2m_N} = \frac{1}{2} \left[ \sqrt{1 + 4\kappa^2} - 1 \right] = \tau_0 = \frac{-Q_0^2}{4m_N^2} > 0. \quad (86)$$

For the RFG one finds that  $-1 < \psi < 1$  and  $\psi = 0$  at the quasielastic peak whose position is given by  $\lambda_0$  (see eq. (77)). The inverse of eq. (84) is given by

$$\lambda = \frac{1}{2} \left[ \sqrt{1 + \left\{ 2\kappa + \psi \sqrt{\xi_F(2 + \xi_F\psi^2)} \right\}^2} - (1 + \xi_F\psi^2) \right] \quad (87)$$

$$= \lambda_0 + \left( \frac{2\kappa}{\sqrt{1 + 4\kappa^2}} \right) \frac{1}{2} \eta_F \psi + \mathcal{O}[\eta_F^2]. \quad (88)$$

The latter also allows us to obtain

$$\tau = \lambda_0 \left[ 1 - \left( \frac{2\kappa}{\sqrt{1 + 4\kappa^2}} \right) \eta_F \psi + \mathcal{O}[\eta_F^2] \right] \quad (89)$$

and these expressions permit us to rewrite eq. (83) in the forms

$$y_{\text{RFG}} = \sqrt{2\xi_F}\psi \left\{ 1 + \frac{1}{2}\xi_F\psi^2 \right\}^{1/2} \quad (90)$$

$$= \frac{m_N}{\kappa} \left\{ \lambda \left[ 1 + \xi_F\psi^2 \right] - \tau \right\} \quad (91)$$

$$= m_N \sqrt{2\xi_F}\psi + \mathcal{O}[\eta_F^2]. \quad (92)$$

The first of these three forms shows that if the reduced response scales with  $\psi$  then it also scales with  $y_{\text{RFG}}$ . Furthermore, from the first and second equations here it is clear that  $y_{\text{RFG}} = 0$  at the QEP where  $\lambda = \lambda_0 = \tau = \tau_0$  and  $\psi = 0$ . Indeed, as the third form shows most clearly, to the extent that we are dealing with dilute systems ( $\eta_F^2 \ll 1$ ) we have that  $y_{\text{RFG}} \cong m_N\eta_F\psi$ .

For comparison, in the  $A \rightarrow \infty$  limit the solution to eqs. (16–17) yields

$$y = 2m_N \left[ \sqrt{\lambda_1(1 + \lambda_1)} - \kappa \right] \quad (93)$$

$$= \frac{m_N}{\kappa(1 + \frac{y}{2q})} [\lambda_1 - \tau_1], \quad (94)$$

where  $\lambda_1 \equiv \lambda - E_S/2m_N$  and  $\tau_1 \equiv \kappa^2 - \lambda_1^2$ . Later (see eq. (123)) we shall introduce the dimensionless energy  $\lambda'$  and thus for completeness we note also that  $\lambda_1 = \lambda' + \xi_F/2$ . For large values of  $q$  at fixed  $y$  (the scaling limit) it is clear that the term  $y/2q$  in eq. (94) may be neglected and that  $y$  has roughly the same form as  $y_{\text{RFG}}$ , except that the peak position is shifted by  $E_S$ , as discussed in ref. [4].

For very light nuclei (very small  $k_F$ ) the distinction between  $y$  and  $y_{\text{RFG}}$  is not very important. Indeed, for extreme cases such as  ${}^3\text{He}$  the most important contributions to the inclusive cross section when not too far from the QE peak arise from a limited region at small  $p$  and small  $\mathcal{E}$ . Hence emphasizing the extreme (and this is used in the definition of  $y$ ; see eqs. (16, 17)) is

reasonable in that case. However, for heavy nuclei important contributions arise from other regions in the  $(p, \mathcal{E})$ -plane. As fig. 7 shows, the RFG concentrates all of its strength along the dotted curve in the figure and therefore the intersection of the kinematic boundary with this curve provides the correct definition (for this model) of what we have called  $y_{\text{RFG}}$  in eq. (83). As we shall see in the next section, models such as the HM distribute the strength still differently and consequently may require definitions of yet other scaling variables. In the present work we limit our attention to  $y$  and  $y_{\text{RFG}}$ , the latter being well-approximated up to multiplicative normalizing constants by  $\psi$ , as well as to a new scaling variable denoted  $\psi'$  to be discussed in the next section.

We complete our review of the RFG by quoting the expression for the inclusive cross section [7]

$$\frac{d^2\sigma}{d\Omega d\epsilon'} = \frac{\mathcal{N}\sigma_M}{4m_N\kappa} S(\psi) \{v_L U_L + v_T U_T\}, \quad (95)$$

where

$$U_L = \frac{\kappa^2}{\tau} (G_E^2 + W_2 \Delta) \quad (96)$$

and

$$U_T = 2\tau G_M^2(\tau) + W_2(\tau), \quad (97)$$

with

$$\begin{aligned} \Delta = \frac{\tau}{\kappa^2} & \left\{ \frac{1}{3} [\epsilon_F^2 + \epsilon_F(1 + \xi_F\psi^2) + (1 + \xi_F\psi^2)^2] \right. \\ & \left. + \lambda [\epsilon_F + (1 + \xi_F\psi^2)] + \lambda^2 \right\} - (1 + \tau). \end{aligned} \quad (98)$$

As usual for the inclusive cross section one should add copies of eq. (95) with  $\mathcal{N} = Z$  and proton form factors to copies with  $\mathcal{N} = N$  and neutron form

factors (see ref. [7]). We shall use generic quantities  $\mathcal{N}$  and  $U_{L,T}$ , although the proton+neutron sums should always be understood.

Worth noting is the analogy between  $U_L$  defined above and  $\mathcal{R}_L$  as given by eq. (51). Their structure is similar: indeed while in  $\mathcal{R}_L$  there appears the factor  $\chi$ , which implies a dependence upon  $p$  and  $\mathcal{E}$ , in  $U_L$  such a factor is replaced by  $\Delta$ , which is constant with respect to these variables. Thus  $U_L$  may be viewed as a suitable average of  $\mathcal{R}_L$  and is a natural ingredient to be used in setting up the reduction factor  $H_L$ , which can only depend on  $q$  and  $\omega$  ( $\kappa$  and  $\lambda$ ). One finds that  $\Delta$ , which does not depend on  $p$  and  $\mathcal{E}$ , in fact depends not only upon  $\kappa$  and  $\lambda$ , but upon the Fermi momentum  $k_F$  as well: it thus still embodies some of the dynamics of the nuclear medium.

The problem of setting up a reduced longitudinal response satisfying the sum rule was solved for the RFG in ref. [8] with the introduction of the following (see eq. (65)):

$$r_L^{\text{RFG}}(q, \omega) = \frac{R_L^{\text{RFG}}(q, \omega)}{H_L^{\text{RFG}}(q, \omega)} \quad (99)$$

with

$$H_L^{\text{RFG}}(q, \omega) = \frac{\mathcal{N}U_L}{J_L}, \quad (100)$$

where

$$J_L \equiv \frac{\kappa\eta_F^3}{2\xi_F}\frac{\partial\psi}{\partial\lambda} = \left(\frac{\eta_F}{\sqrt{2\xi_F}}\right)^3 \sqrt{1 + \frac{1}{2}\xi_F\psi^2} \left(\frac{\kappa^2}{\tau}\right) \left[\frac{1 + 2\lambda + \xi_F\psi^2}{1 + \lambda + \xi_F\psi^2}\right] \quad (101)$$

$$= \left(\frac{\kappa^2}{\tau}\right) \left[\frac{1 + 2\lambda}{1 + \lambda}\right] + \mathcal{O}[\eta_F^2]. \quad (102)$$

As usual here, the generic form  $\mathcal{N}U_L$  is used whereas the actual result must have  $ZU_{Lp} + NU_{Ln}$ . A little algebra then yields

$$r_L^{\text{RFG}}(q, \omega) = \frac{3}{8m_N}(1 - \psi^2)\theta(1 - \psi^2)\frac{\partial\psi}{\partial\lambda}, \quad (103)$$

whose moments

$$\Xi_n^{\text{RFG}}(q) = \int_0^\infty d\omega r_L^{\text{RFG}}(q, \omega) \lambda^n \quad (104)$$

are then easily evaluated using eq. (87), which may be simplified when  $\kappa \gg \xi_F$  to the expression in eq. (88). One then immediately gets for the moments

$$\Xi_0^{\text{RFG}} = 1 \quad (\text{sum rule}) \quad (105)$$

$$\Xi_1^{\text{RFG}} \simeq \lambda_0 \quad (\text{mean energy}) \quad (106)$$

$$\Xi_2^{\text{RFG}} \simeq \lambda_0^2 + \frac{1}{5} \frac{\kappa^2 \eta_F^2}{(1 + 4\kappa^2)}. \quad (107)$$

Finally, the variance of the RFG is then obtained according to

$$\sigma^{\text{RFG}} = \sqrt{\Xi_2^{\text{RFG}} - (\Xi_1^{\text{RFG}})^2} \simeq \frac{1}{2\sqrt{5}} \frac{1}{m_N} \frac{qk_F}{\sqrt{q^2 + m_N^2}} = \frac{1}{\sqrt{5}} \frac{\kappa \eta_F}{\sqrt{1 + 4\kappa^2}}. \quad (108)$$

Having revisited the basics of the RFG and established in the RFG framework the connection, for  $q > 2k_F$ , between inclusive and exclusive scattering, in the next section we shall set up a more realistic spectral function that in particular accounts for the confinement of the nucleons in the initial state.

## 6 The hybrid model

In this section we derive a spectral function that accounts for the confinement of the nucleons inside the nucleus in its initial state employing a simple, tractable model where the  $A \rightarrow \infty$  limit may be relatively easily performed. The initial state is viewed as an assembly of independent particles moving non-relativistically in a harmonic oscillator well, namely

$$H_{HO} = \frac{p^2}{2m_N} + \frac{1}{2} m_N \omega_0^2 r^2 - (N_{\max} + 3/2) \omega_0 - E_S. \quad (109)$$

The constant terms in the above set the energy scale in such a way that the energy required to remove a nucleon from the outermost shell just corresponds to the separation energy  $E_S$ . In the following  $N = 2n + \ell$  is the principal quantum number of an occupied shell and  $N_{\max}$  the highest value of  $N$ . The energies of the excited state of the daughter nucleus are

$$M_{A-1} = M_A^0 - m_N - (N - N_{\max})\omega_0 + E_S \quad (110)$$

and the excitation energy of the residual nucleus, measured with respect to the ground state and in a frame where it is moving with momentum  $-\mathbf{p}$ , are

$$\begin{aligned} \mathcal{E}^{\text{HM}} &= \sqrt{p^2 + (M_{A-1})^2} - \sqrt{p^2 + (M_{A-1}^0)^2} \\ &\cong \frac{p^2}{2M_{A-1}} + M_{A-1} - \frac{p^2}{2M_{A-1}^0} - M_{A-1}^0 \\ &\cong (N_{\max} - N)\omega_0, \end{aligned} \quad (111)$$

where the recoil energy of the daughter nucleus has been neglected in the last expression.

In the same approximation the spectral function reads

$$\tilde{S}^{\text{HM}}(\mathbf{p}, \mathcal{E}) = \sum_{N=0}^{N_{\max}} \delta[\mathcal{E} - (N_{\max} - N)\omega_0] n_N(p), \quad (112)$$

where  $n_N(p)$  is the momentum distribution of the  $N^{\text{th}}$  shell of the considered nucleus, *i.e.*

$$n_N(p) = \sum_{\substack{n, \ell \\ (2n+\ell=N)}} |\varphi_{n\ell}(p)|^2 \sum_{m=-\ell}^{\ell} |Y_{\ell,m}(\hat{\mathbf{p}})|^2 = \sum_{\substack{n, \ell \\ (2n+\ell=N)}} \frac{2\ell+1}{4\pi} |\varphi_{n\ell}(p)|^2, \quad (113)$$

the radial harmonic oscillator wave functions in momentum space being related to the corresponding quantities in coordinates space  $R_{n\ell}$  by ( $\nu = m_N\omega_0$ )

$$\varphi_{n\ell}(p) = \sqrt{\frac{1}{\nu^3}} R_{n\ell} \left( \frac{p}{\nu} \right). \quad (114)$$

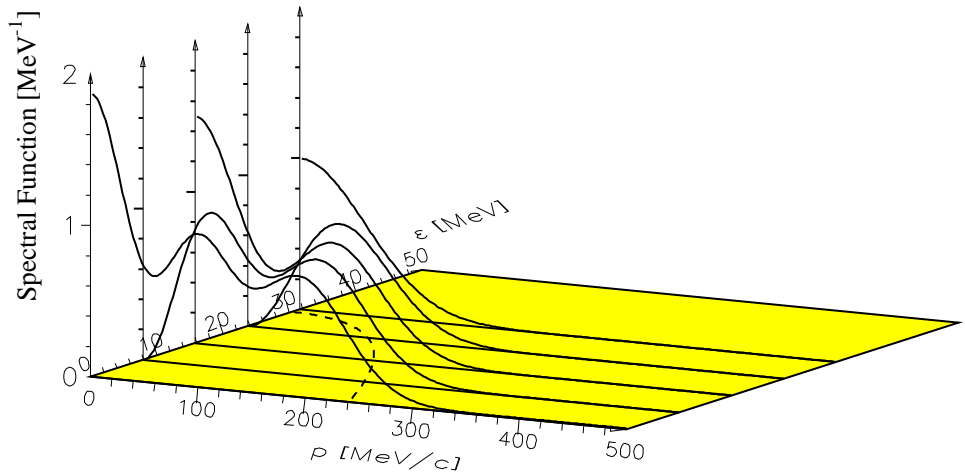


Figure 8: The spectral function in  $\text{MeV}^{-1}$  using harmonic oscillator wave functions for the ( $N = Z$ ) nucleus  $A = 140$  ( $N_{\text{max}} = 4$ ) with  $\omega_0 = 7.9$  MeV. Also displayed is the support of the  $\tilde{S}^{\text{RFG}}$  for  $k_F = 1.112 \text{ fm}^{-1}$ . The latter confines the former, but for a small leakage, in a corner of the  $(\mathcal{E}, p)$  plane. Also shown is the kinematically allowed domain for the exclusive process for  $q = 300 \text{ MeV}/c$  and  $\omega = 25 \text{ MeV}$ .

Analytic expressions may be obtained for these quantities, although for the sake of brevity these are not given here. The support in the  $(\mathcal{E}, p)$  plane of the harmonic oscillator spectral function  $\tilde{S}^{\text{HM}}(\mathbf{p}, E)$  is a set of lines, one for each shell  $N$  of the daughter nucleus, all parallel to the  $p$ -axis. It is displayed in figs. 7 and 8 for  $N_{\text{max}} = 4$ , which would correspond to the nucleus  $^{140}\text{Yb}$ , together with the region kinematically accessible to a semi-inclusive process for a choice of values of  $\omega$  and  $q$  yielding a positive  $y$ . Also shown in the same figures is the corresponding curve from eq. (74) for the RFG for  $k_F = 1.112 \text{ fm}^{-1}$ .

The two supports of the spectral functions displayed in figs. 7 and 8 are indeed very different: the dramatic difference between  $\tilde{S}^{\text{RFG}}$  and  $\tilde{S}^{\text{HM}}$  is fully apparent and it should not be surprising that the RFG and HM models yield drastically different predictions for exclusive processes. One would like to fix  $k_F$  in such a way that the points where the support of the RFG spectral function crosses that of the harmonic oscillator HM coincide with the root-mean-square value of the momentum  $p$  in the corresponding shell. For the harmonic oscillator the root-mean-square (r.m.s.) momentum in a given shell reads

$$\sqrt{\langle p^2 \rangle_N} = \sqrt{m_N \omega_0 \left( N + \frac{3}{2} \right)}. \quad (115)$$

Therefore eq. (111) can be recast as follows

$$\mathcal{E}^{\text{HM}} = (N_{\text{max}} - N) \omega_0 = \left( N_{\text{max}} + \frac{3}{2} \right) \omega_0 - \frac{\langle p^2 \rangle_N}{m_N} \quad (116)$$

and then compared with the Fermi gas expression in the non-relativistic limit (see eq. (74))

$$\mathcal{E}^{\text{RFG}} = \frac{k_F^2}{2m_N} - \frac{p^2}{2m_N}, \quad (117)$$

viewing  $\langle p^2 \rangle_N$  as a continuous variable. Owing to the factor  $\frac{1}{2}$  in front of the term  $p^2/m_N$  in eq. (117) one immediately realizes that no choice of  $\omega_0$  and  $k_F$  can reconcile eqs. (116) and (117).

For a chosen  $\omega_0$  it is possible, however, by equating eqs. (116) and (117) to determine a Fermi momentum  $k_F^N$  such that the r.m.s. momentum in a given shell of the harmonic oscillator is identical to the Fermi gas value. One obtains

$$k_F^N = \sqrt{m_N \omega_0} \sqrt{2N_{\max} - N + \frac{3}{2}}, \quad (118)$$

which implies that the inner (outer) shells of a nucleus are related to a Fermi gas with a larger (lower) density, respectively.

Quantitatively we illustrate this relation by displaying in table 1 the values of  $k_F^N$  for all the shells of six different nuclei ( $\omega_0 = 41/A^{1/3}$  MeV), where in our “toy model” only  $N = Z$  nuclei are considered.

In heavy nuclei the  $k_F$  associated with the innermost shell ( $N = 0$ ) are indeed close to the nuclear matter value  $k_F^{nm} = 1.36 \text{ fm}^{-1}$  whereas the outer shells relate to values of  $k_F$  which are about 30% lower than  $k_F^{nm}$ ; hence the correspondence between  $k_F$  and  $\nu$ , or better, between the density and the size of a nucleus, can only be established on the average. For example one might define for each nucleus an average Fermi momentum according to

$$\bar{k}_F = \sqrt{\frac{\sum_{N=0}^{N_{\max}} (N+1)(N+2)(k_F^N)^2}{\sum_{N=0}^{N_{\max}} (N+1)(N+2)}}, \quad (119)$$

$k_F^N$  being given by eq. (118).

The values of the Fermi momentum thus obtained are reported in table 1 and displayed as a function of the mass number  $A$  in fig. 9 where it is seen that the nuclear matter value of  $1.36 \text{ fm}^{-1}$  will just be reached for the innermost shells of very heavy nuclei. Note also that when available from

N	$^{16}\text{O}$	$^{40}\text{Ca}$	$^{80}\text{Zr}$	$^{140}\text{Yb}$	$^{224}\text{?}$	$^{336}\text{?}$
0	1.172	1.261	1.312	1.345	1.368	1.385
1	0.990	1.140	1.221	1.272	1.307	1.333
2		1.006	1.123	1.195	1.243	1.279
3			1.016	1.112	1.176	1.222
4				1.023	1.105	1.162
5					1.029	1.099
6						1.033
$k_F$	1.039	1.075	1.097	1.112	1.123	1.131
$\alpha_F$	1.18	1.12	1.10	1.09	1.09	1.09

Table 1: The Fermi momenta (all in  $\text{fm}^{-1}$ ) associated with each shell  $N$  of the harmonic oscillator. In the next-to-last row the Fermi momentum averaged according to eq. (119) is given. The final row gives the quantity  $\alpha_F$  defined in eq. (129).

the width of the quasi-elastic peak as measured in inclusive inelastic electron scattering the experimental values of  $k_F$  appear to be typically about 20% higher than those predicted by eq. (119). The curve labelled  $\bar{k}_F'$  is discussed later.

Let us now compare the spectral function of the HM with that of the RFG, which should be viewed as a  $\delta$ -function with its base lying on the support curve of  $\tilde{S}^{\text{RFG}}$ . They are displayed in fig. 8 for the nucleus  $A = 140$  and for  $k_F = 1.112 \text{ fm}^{-1}$ .

Once the spectral function is given – see eq. (112) – we obtain the longitudinal response from eq. (40),

$$R_L^{\text{HM}}(q, \omega) = \frac{2\pi}{q} \sum_{N=0}^{N_{\max}} \int dp d\mathcal{E} p n_N(p) \frac{m_N^2}{E(\mathbf{p})} \mathcal{R}_L(q, \omega, p, \mathcal{E}) \delta[\mathcal{E} - (N_{\max} - N) \omega_0], \quad (120)$$

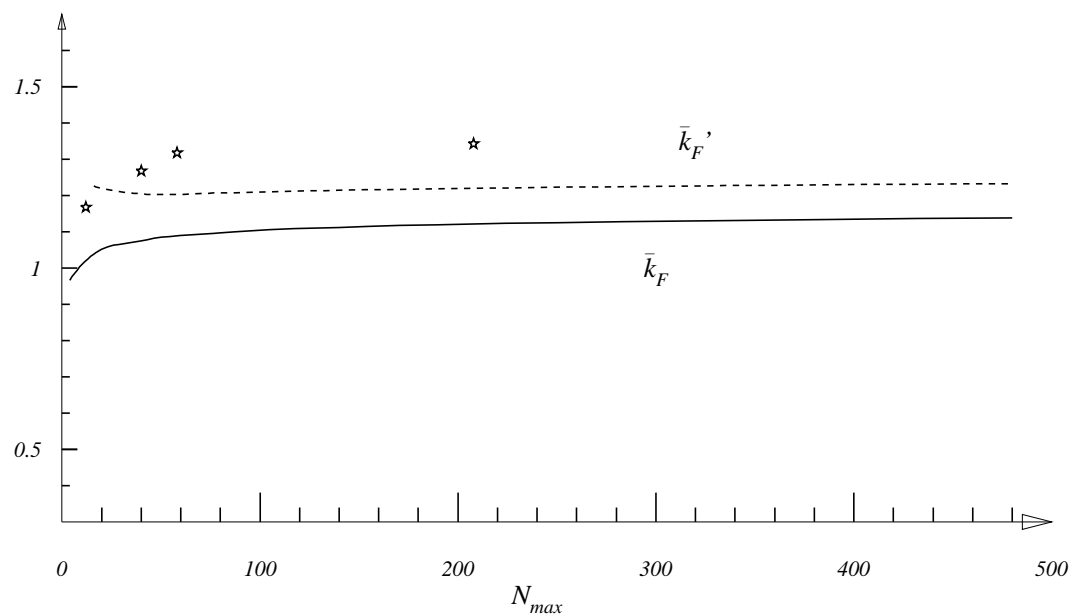


Figure 9: Values of  $\bar{k}_F$  and  $\bar{k}_F'$  (in  $\text{fm}^{-1}$ ) as defined by eqs. (119) and (128), respectively, versus  $N_{\max}$ . A few experimental values for nuclei with the same mass numbers are also shown.

which should be divided by an appropriate reduction factor as in eq. (66) to obtain the sum rules. In this connection the problem of the off-shellness of the single-nucleon response still has to be faced. In fact only for the RFG has a reduction factor, namely the  $H_L$  in eq. (100), been obtained.

We begin by noting that in general  $\mathcal{R}_L$  depends upon the variables  $p$  and  $\mathcal{E}$  because the initial nucleon is not at rest and is off-shell, although in a low-density regime (as for nuclear matter) such a dependence is expected to be mild. Moreover, since for a finite nucleus the momentum distribution is also concentrated in a rather restricted region, in fact mostly within the Fermi sphere, and the tail contribution is quite small, it might appear to be justified to assume the same reduction factor of the RFG, namely  $H_L^{\text{RFG}}(q, \omega)$ , for the hybrid model as well.

A delicate point relates however to the energy scales of the RFG and of the hybrid model.

Both are set by the separation energy  $E_S$ , but as discussed above in the RFG case the latter is negative ( $-T_F$ , where  $T_F = \sqrt{m_N^2 + k_F^2} - m_N$  is the kinetic energy of a particle at the Fermi surface) while for the harmonic oscillator the separation energy has been chosen to be positive, as it is for real nuclei. This forces the struck nucleon off-shell according to eq. (11) — recall that  $E$  is the correct (*i.e.*, off-shell) energy of the struck nucleon, whereas  $\overline{E}$  in eq. (10) is the corresponding on-shell quantity for the same three-momentum  $p$ .

In our treatment using the HM we make two assumptions. First, we ignore the daughter nucleus recoil energy,  $T_{A-1}^0 \cong p^2/2M_{A-1}^0$ , in eq. (11). Since typically  $p$  is less than  $k_F$  where the spectral function plays a significant role and since our focus is on medium-weight nuclei (in fact, one of our goals

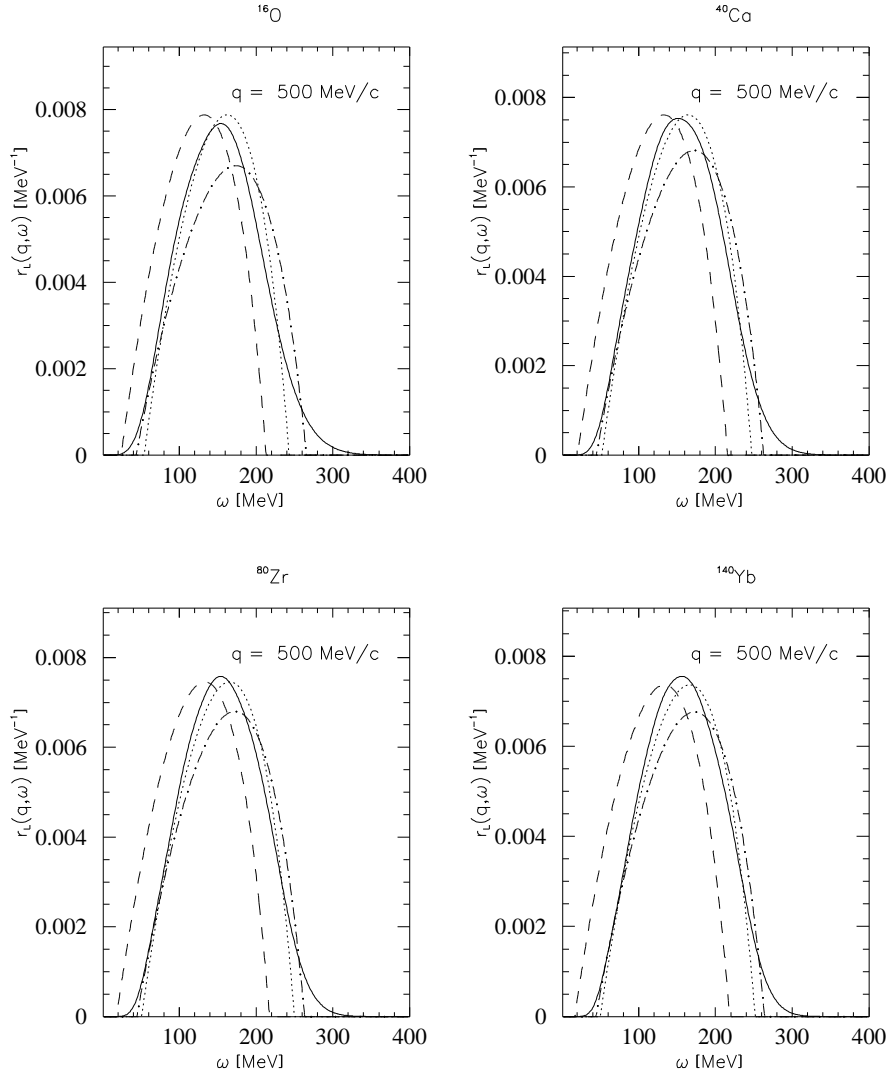


Figure 10: Longitudinal reduced responses for different nuclei at  $q = 500$  MeV/c. Dashed lines: RFG, with  $k_F$  evaluated according to eq. (119); dotted lines: RFG, with  $k_F$  evaluated according to eq. (119) and the energy shift suggested in eq. (123); dash-dotted lines: RFG, with the energy shift in eq. (123) as well as with the scaled Fermi momentum given by eq. (128); solid lines: hybrid model.

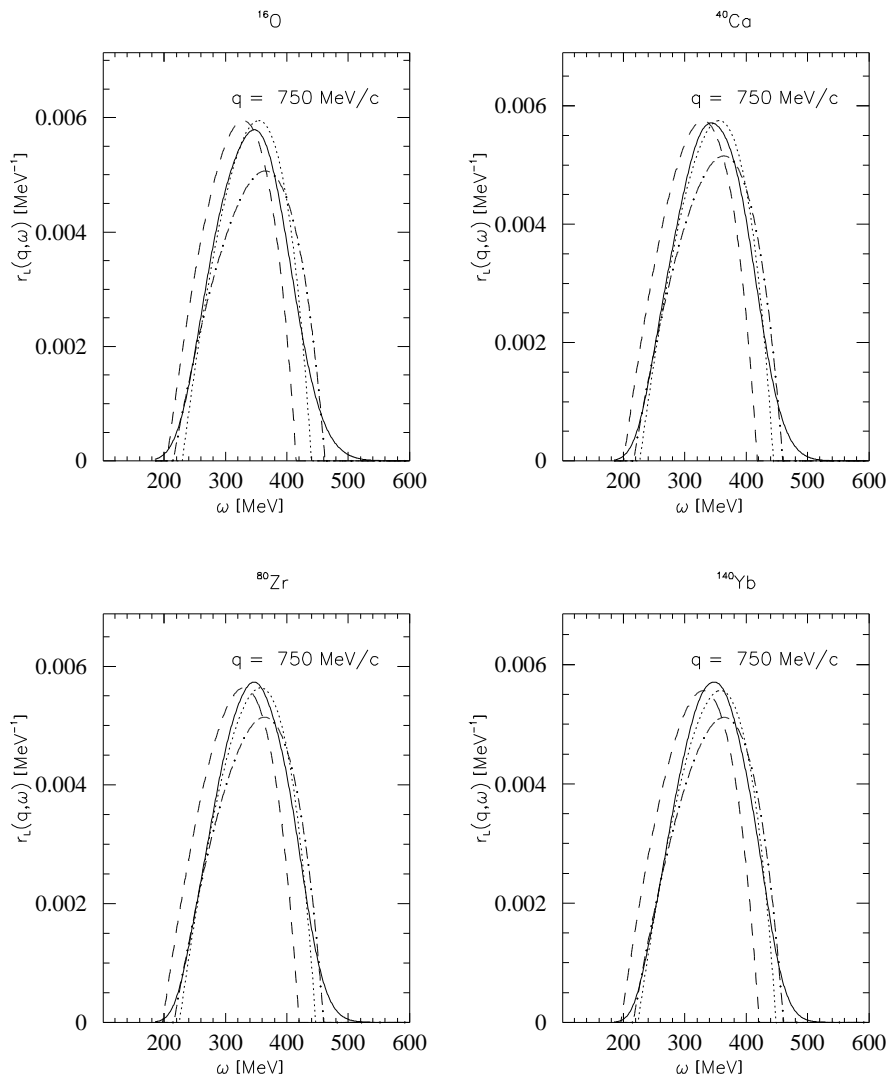


Figure 11: Same as fig. 10, but for  $q = 750$  MeV/c

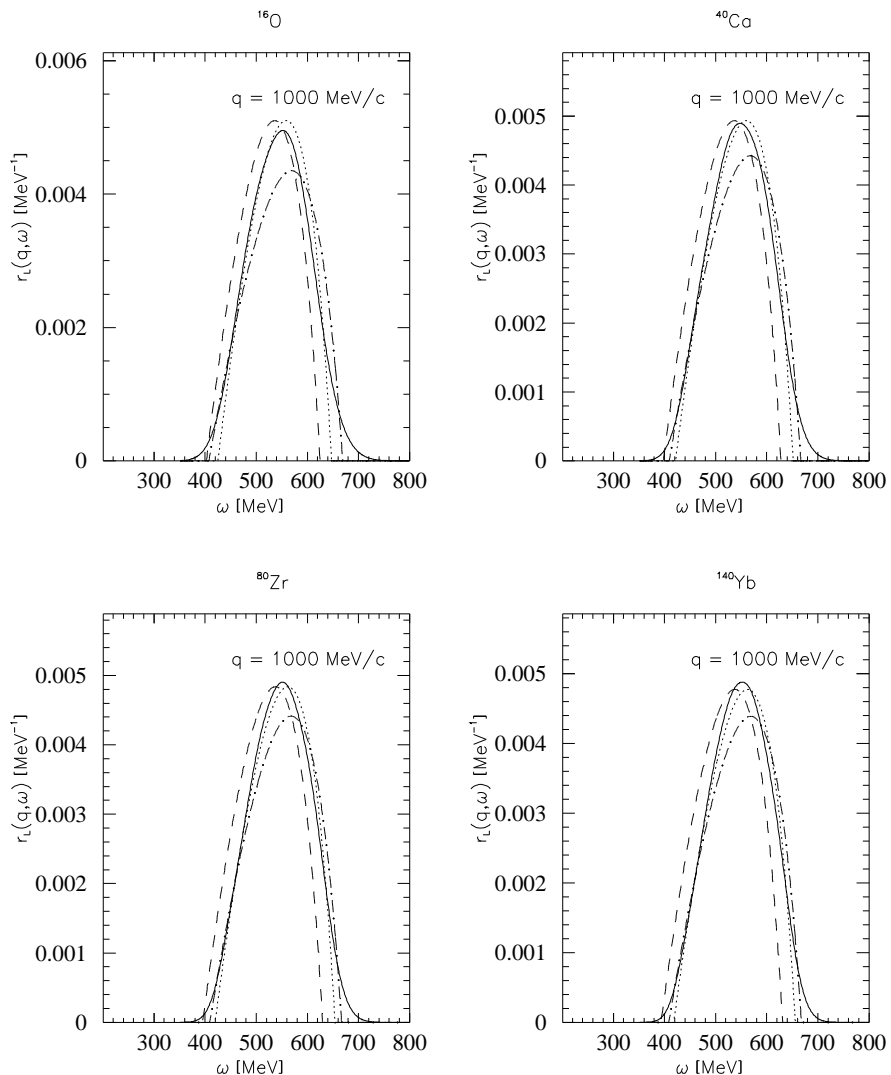


Figure 12: Same as fig. 10, but for  $q = 1000$  MeV/c

has been to develop inter-model comparisons in the limit where  $A \rightarrow \infty$ ), dropping this energy amounts to an error of less than an MeV under typical circumstances. Of course, for very light nuclei or for very large missing momenta one should be more careful with this contribution.

Second, in determining the reduction factor  $H_L^{\text{HM}}(q, \omega)$ , which should only depend on  $q$  and  $\omega$ , we use instead of the full variation in  $\mathcal{E}$  only the “average value” provided by the RFG as given in eq. (74). We then have

$$\begin{aligned} \mathcal{E} + \overline{E} - m_N &\rightarrow \mathcal{E}^{\text{RFG}} + \overline{E} - m_N \\ &= T_F = -E_S^{\text{RFG}} \end{aligned} \quad (121)$$

and then eq. (11) yields

$$\overline{E} - E \rightarrow E_S + T_F = E_S - E_S^{\text{RFG}} \quad (122)$$

or, using eq. (53),

$$\overline{\omega} \rightarrow \omega' \equiv \omega - [E_S - E_S^{\text{RFG}}], \quad (123)$$

and  $\lambda' \equiv \omega'/2m_N$ ; also  $\overline{\tau}$  is then given by eq. (54) so that  $\overline{\tau} \rightarrow \tau' \equiv \kappa^2 - \lambda'^2$ . Furthermore, in analogy with eq. (84), we also define a “shifted” scaling variable:

$$\psi' \equiv \frac{1}{\sqrt{\xi_F}} [2\theta(\lambda' - \lambda_0) - 1] \left\{ \sqrt{(1 + \lambda')^2 + \frac{1}{\tau'}(\tau' - \lambda')^2} - (1 + \lambda') \right\}^{1/2}. \quad (124)$$

We note in passing that it appears [9] that quasielastic data taken at intermediate energies in fact scale somewhat better when  $r_F(q, \omega)$  is plotted as a function of  $\psi'$  than when plotted versus either  $\psi$  or  $y$ . The new reduction factor, denoted  $H_L(q, \omega; E_S)$ , is then obtained from an extension of eq. (100) to account for the off-shell nature of the EM vertex:

$$H_L(q, \omega; E_S) = \frac{\mathcal{N}U_L^{\text{off}}}{J_L^{\text{off}}}, \quad (125)$$

where  $J_L^{\text{off}}$  is given by eqs. (101,102) with the above replacements of  $\lambda \rightarrow \lambda'$  and  $\tau \rightarrow \tau'$  together with the CC1/CC2 form for the longitudinal projection of the off-shell EM current,

$$\begin{aligned} U_L^{\text{off}} = & \frac{\kappa^2}{\tau} \left[ \left\{ G_E^2 + \frac{1}{\tau'} (\tau - \tau') [F_1^2 - \tau \tau' F_2^2] \right\} \right. \\ & \left. + \left\{ W_2 + \frac{1}{\tau'} (\tau - \tau') F_1^2 \right\} \Delta(\lambda \rightarrow \lambda', \tau \rightarrow \tau') \right] \end{aligned} \quad (126)$$

with  $\Delta$  given by eq. (98) after replacement to primed variables. As usual  $\mathcal{N}U_L^{\text{off}}$  should be taken to mean  $ZU_{Lp}^{\text{off}} + \mathcal{N}U_{Ln}^{\text{off}}$ . Note that  $H_L(q, \omega; E_S)$  reverts to the on-shell answer in eq. (100) when  $E_S = E_S^{\text{RFG}}$ .

Having fixed the definition of  $H_L(q, \omega; E_S)$  the reduced response and the sum rules can be evaluated numerically. We display the HM reduced charge response in figs. 10-12 for  $q = 500, 750$  and  $1$  GeV respectively (solid curves). In the figures the  $E_S$  of the HM is set to  $8$  MeV and the  $k_F$  of the RFG is fixed according to eq. (119).

The basic features of the HM reduced response (as compared to that of the RFG shown as dashed curves) emerging from the present analysis are:

- i) an upward shift in energy,
- ii) “tails” at high and low  $\omega$ , and
- iii) a somewhat larger half-width (see below).

All of these traits were of course to be expected and are easily understood: indeed it is harder to pull nucleons out of a system when they are bound, hence the shift in energy, and confined nucleons have distributions extending to higher momenta because of the uncertainty principle, hence the larger width and tails of the HM charge response. Notably these features appear

to be largely unaffected by the momentum transferred to the nuclear system at least in the range up to 1 GeV.

Both the upward shift and the broadening of the response are seen even more clearly in figs. 13, 14 and 15 where the normalized sum rule, energy-weighted sum rule (EWSR) and variance  $\sigma$  of the HM and RFG are displayed.

With respect to the Coulomb sum rule of the HM shown in fig. 13 we first notice that a small deviation from one at large  $q$  might be expected, since a low-density approximation was employed in deriving the reduction factor, although such a deviation never exceeds 1-2%.

Second, to help in appreciating the role of confinement, we display together with the HM results three different versions of the RFG sum rule. Thus in the figure the solid lines correspond to the case in which the integration is performed from  $\omega = 0$  up to the light cone (non-Pauli-blocked RFG), while for the dotted lines the integration starts from the RFG separation energy. In this last instance the sum rule receives contributions even from negative values of  $\omega$ , since in fact the threshold energy in the RFG is negative (namely  $E_S$ ).

Finally the dash-dotted lines correspond to the RFG sum rule with the Pauli principle included and the integration ranging from  $\omega = 0$  up to the light cone. A comparison of the dotted and solid lines (hybrid model) shows the impact of the confinement, insofar as the former rises vertically at threshold, while confinement smooths out the approach to the asymptotic sum rule. This behaviour is further softened by the action of the Pauli principle, as reflected in the dash-dotted lines.

An interesting relationship can be established with respect to the EWSR

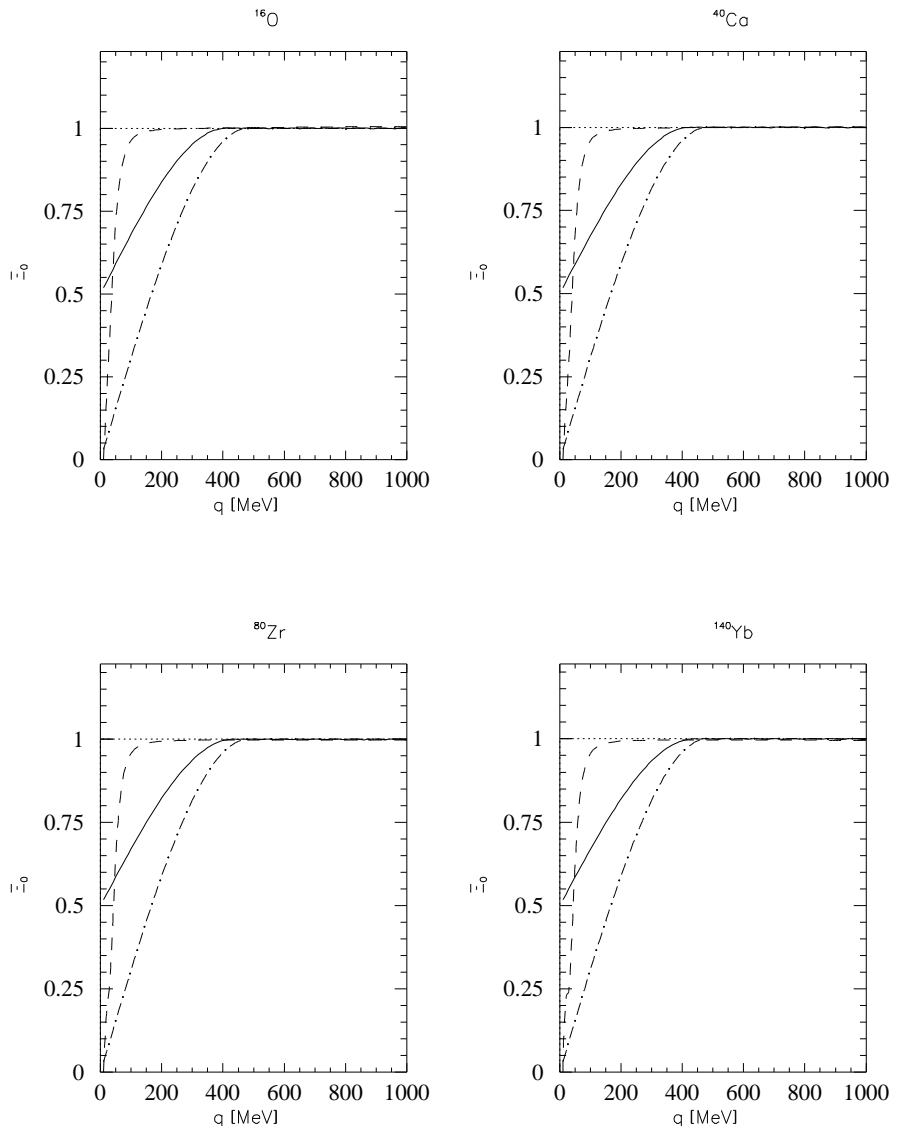


Figure 13: The normalized Coulomb Sum Rule. Solid lines: non-Pauli-blocked RFG with integration from 0 to  $q$ ; dotted lines: non-Pauli-blocked RFG with integration from  $E_S$  to  $q$ ; dash-dotted lines: RFG with integration from 0 to  $q$  and with the inclusion of the Pauli principle; dashed lines: hybrid model.

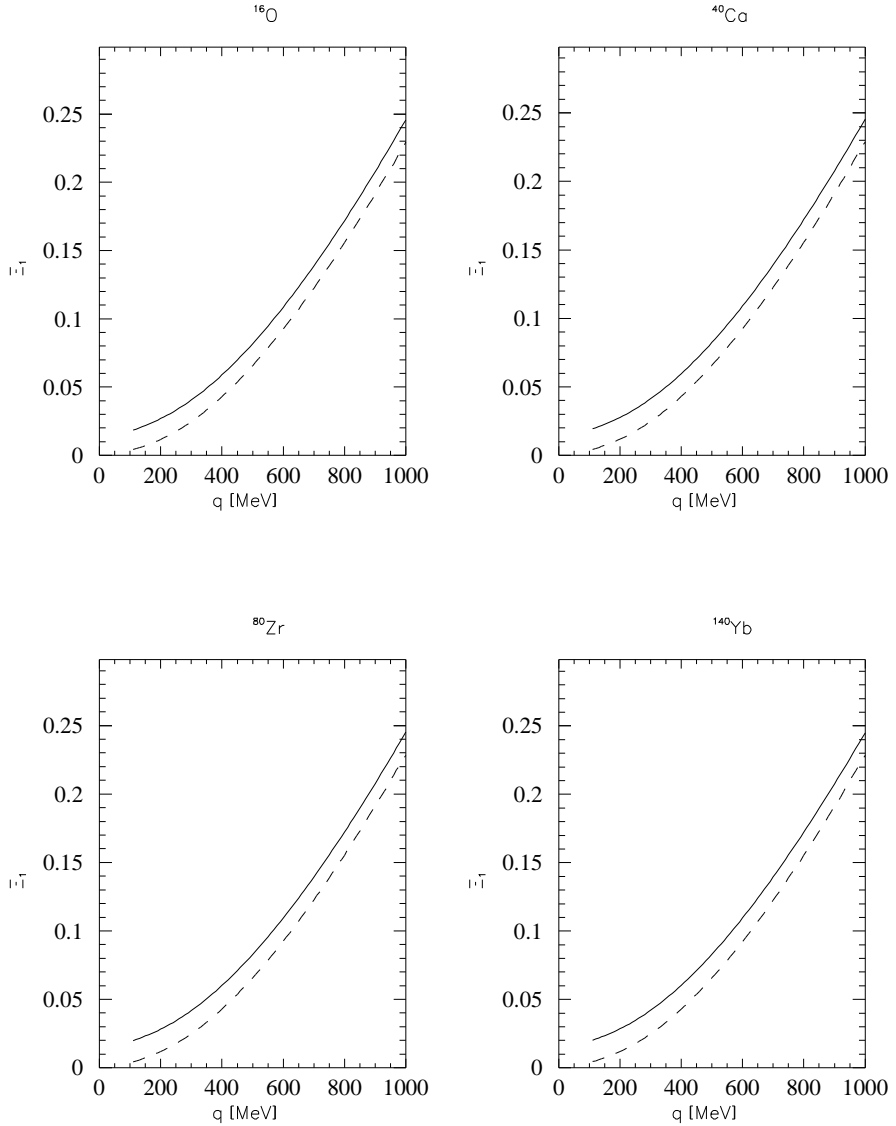


Figure 14: The normalized energy-weighted sum rule. Dashed lines: RFG, with  $k_F$  evaluated according to eq. (119); solid lines: RFG with  $k_F$  evaluated according to eq. (119) together with the energy shift suggested in eq. (123) or RFG with the energy shift in eq. (123) as well as with the scaled Fermi momentum given by eq. (128) or hybrid model (the last three yield a single result).

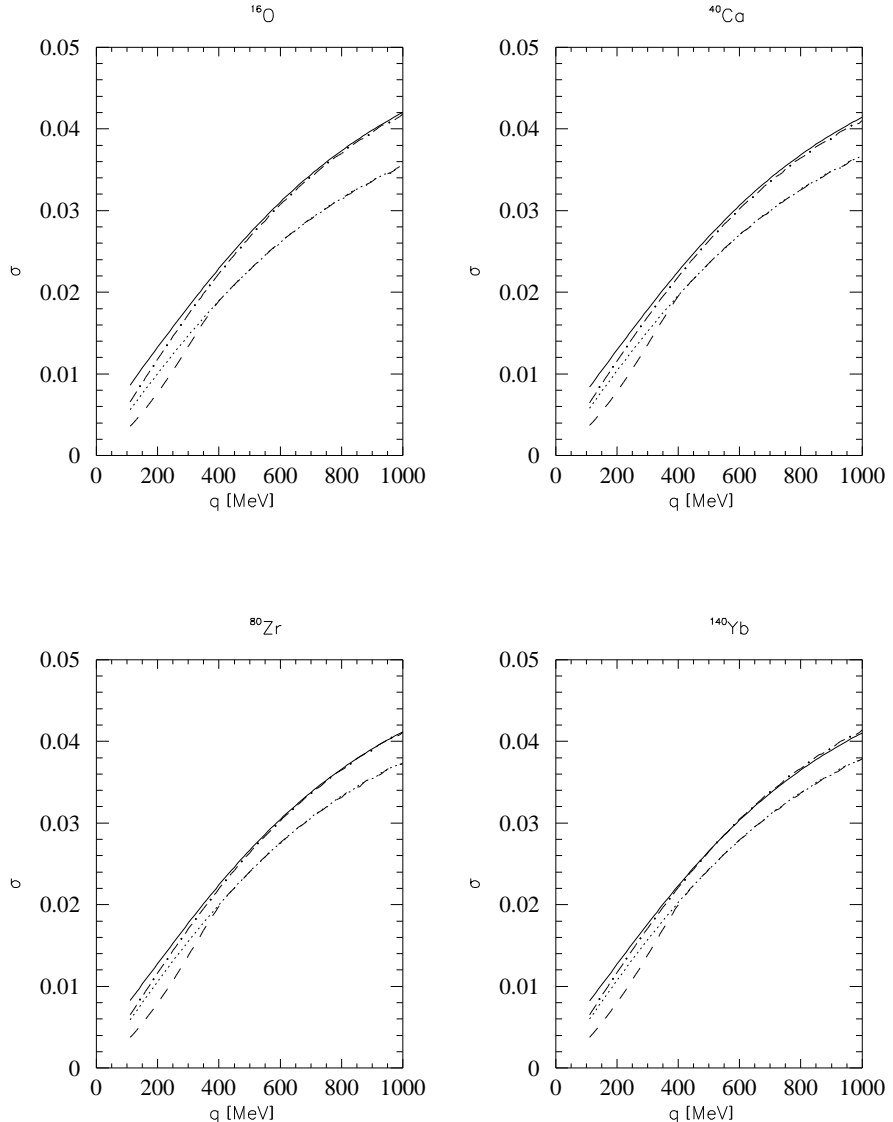


Figure 15: The variance  $\sigma$ . Dashed lines: RFG, with  $k_F$  evaluated according to eq. (119); dotted lines: RFG, with  $k_F$  evaluated according to eq. (119) and the energy shift suggested in eq. (123); dash-dotted lines: RFG, with the energy shift in eq. (123) as well as with the scaled Fermi momentum given by eq. (128); solid lines: hybrid model.

	$E_S = -T_F$					$E_S = 8 \text{ MeV}$			
$q \text{ (GeV/c)}$	0.5	1	1.5	2	$q \text{ (GeV/c)}$	0.5	1	1.5	2
$^{16}\text{O}$	0.02	-0.86	-1.43	-1.31	$^{16}\text{O}$	-0.35	-1.39	-2.13	-2.10
$^{40}\text{Ca}$	-0.03	-0.34	-0.87	-1.19	$^{40}\text{Ca}$	-0.38	-0.88	-1.58	-2.00
$^{80}\text{Zr}$	0.02	-0.12	-0.56	-1.11	$^{80}\text{Zr}$	-0.33	-0.67	-1.29	-1.94
$^{140}\text{Yb}$	0.08	-0.16	-0.36	-1.06	$^{140}\text{Yb}$	-0.26	-0.72	-1.10	-1.90
$^{224}\text{?}$	0.15	-0.10	-0.22	-0.63	$^{224}\text{?}$	-0.19	-0.67	-0.97	-1.48
$^{336}\text{?}$	0.21	-0.06	-0.12	-0.31	$^{336}\text{?}$	-0.13	-0.64	-0.88	-1.17
	$E_S = 30 \text{ MeV}$					$E_S = 50 \text{ MeV}$			
$q \text{ (GeV/c)}$	0.5	1	1.5	2	$q \text{ (GeV/c)}$	0.5	1	1.5	2
$^{16}\text{O}$	-0.73	-1.90	-2.74	-2.75	$^{16}\text{O}$	-1.22	-2.45	-3.36	-3.40
$^{40}\text{Ca}$	-0.75	-1.37	-2.17	-2.64	$^{40}\text{Ca}$	-1.22	-1.91	-2.78	-3.27
$^{80}\text{Zr}$	-0.69	-1.16	-1.87	-2.57	$^{80}\text{Zr}$	-1.15	-1.69	-2.47	-3.19
$^{140}\text{Yb}$	-0.62	-1.20	-1.68	-2.52	$^{140}\text{Yb}$	-1.08	-1.73	-2.28	-3.14
$^{224}\text{?}$	-0.55	-1.15	-1.55	-2.11	$^{224}\text{?}$	-1.01	-1.68	-2.15	-2.73
$^{336}\text{?}$	-0.49	-1.12	-1.46	-1.79	$^{336}\text{?}$	-0.95	-1.65	-2.06	-2.41

Table 2: The difference between left- and right-hand sides of eq. (127) in MeV. The RFG is taken with  $k_F$  defined by eq. (119).

shown in fig. 14: the EWSR quantifies the location of the maximum of the response, which in turn, as we have seen, occurs in the proximity of the energy where the scaling variable vanishes. On the basis of eq. (123) it is therefore natural to expect the following relationship to hold for the energy-weighted sum-rule difference (EWSRD):

$$2m_N \left[ \frac{\Xi_1^{\text{HM}}}{\Xi_0^{\text{HM}}} - \frac{\Xi_1^{\text{RFG}}}{\Xi_0^{\text{RFG}}} \right] = T_F + E_S. \quad (127)$$

Indeed in table 2, where  $k_F$  is chosen in accord with eq. (119), one sees eq. (127) to be very well obeyed for a number of nuclei, over a large span of momentum transfers and for several choices of the separation energy. Actually the departures from the predictions of eq. (127), while mild, tend to grow with  $q$ , a symptom of their relativistic origin. However they stay very small even for unreasonable large separation energies.

With these ideas in mind we show as dotted curves in figs. 10–12, 14, 15 the result of shifting the RFG answers by  $E_S + T_F$ , that is, using  $\omega'$  in eq. (123) to replace  $\omega$  (this implies that  $\lambda \rightarrow \lambda'$  and  $\tau \rightarrow \tau'$ , as discussed above, everywhere except in the single-nucleon form factors where  $\tau$  is retained). Clearly this produces roughly the correct shift to yield agreement with the HM results. The EWSR shown as a dotted curve in fig. 14 now approximates the HM answer, whereas the variance in fig. 15 is largely unaffected by the shift.

This last observation suggests the strategy of modifying the Fermi momentum from the results given by eq. (119) with the hope of adjusting the variance so that the “renormalized” RFG model has the same value of  $\sigma$  as the HM and yet at the same time has the shift discussed above. Since the EWSR and variance are primarily affected by the shift and scaled Fermi momentum, respectively, in an almost “orthogonal” way, we anticipate being able to obtain agreement for all of the first three energy-weighted moments. Thus, in figs. 10–12, 14, 15 we also show as dash-dotted curves results where the shift by  $E_S + T_F$  discussed above is performed and as well where the Fermi momentum is scaled according to

$$\bar{k}_F' \equiv \alpha_F \bar{k}_F, \quad (128)$$

where  $\alpha_F$  is the dimensionless factor required to make this renormalized RFG model have the same variance as the HM. In table 1 we give the values of  $\alpha_F$  required to accomplish this; they are found to obey the relationship

$$\alpha_F = 1.08 + \frac{1.6}{A} \quad (129)$$

reasonably well. The resulting values of  $\bar{k}_F'$  are shown in fig. 9 where it is clear that the trend is in the right direction, the data now falling only about

10% higher than the scaled Fermi momenta for heavy nuclei.

We deduce from this that the “Fermi momentum” one uses in other applications of the RFG should be viewed with some caution. If only properties of the  $A$ -body nuclear ground state and of low-lying states in the  $A - 1$  daughter nucleus are used to fix the effective Fermi momentum (as in the present work when spectral functions of RFG and HM are compared), then one value emerges, namely  $\bar{k}_F$ . In contrast, when cognizance is taken of the full  $A$ -body final nuclear state with a nucleon far up in the continuum by using the QE responses in a model-to-model comparison, then a larger effective Fermi momentum,  $\bar{k}_F'$ , is found. Even extrapolating to  $A = \infty$  still produces an 8% upward scaling.

## 7 Conclusions

In the present work we have achieved the goals set out in the Introduction. First, we have succeeded in deriving the non-Pauli-blocked RFG directly from the PWIA by constructing covariant initial and final (non-interacting) nuclear states, and from these obtaining the RFG spectral function. We have used the deepened understanding that comes from this approach to re-examine the issues of defining a reduced response function with its attendant properties,  $y$ -scaling,  $\psi$ -scaling and energy-weighted moments including the zeroth moment or Coulomb sum rule.

The second general goal of the present work was to develop a simple, tractable model for the nuclear spectral function that incorporates the confinement of nucleons in the initial state. Our specific model, a hybrid model with harmonic oscillator wave functions, is designed in a way that facilitates taking the  $A \rightarrow \infty$  with minimal numerical effort. From comparisons

between the HM and RFG spectral functions it is possible to define an average Fermi momentum  $\bar{k}_F$  and to examine its behaviour in the large- $A$  limit. Typically the value obtained falls below that extracted from experimental determinations using QE scattering by roughly 20%, and only for the innermost shells of very heavy nuclei is the standardly accepted nuclear matter Fermi momentum reached.

Further comparisons of HM and RFG through reduced response functions and the resulting energy-weighted sum rules tell us that the global nature of the spectral functions is quite similar for the two models, although the detailed distribution in missing energy and missing momentum is not. As a consequence, while inclusive lepton scattering responses turn out to be similar, for exclusive scattering the models would yield radically different results, as expected. In particular, the definition of the reduced inclusive longitudinal response requires a reduction factor  $H_L$  which can be model dependent and so render the various energy-weighted sum rules, including importantly the Coulomb sum rule, model dependent. We find, however, that  $H_L^{\text{RFG}}$  and  $H_L^{\text{HM}}$  are only very weakly model dependent. The former proceeds from the on-shell single-nucleon current whereas the latter starts from off-shell prescriptions for the single-nucleon current, and yet, when the differing kinematics in the two models are correctly incorporated, the final results are almost indistinguishable. This bodes well for studies of scaling and energy-weighted moments for then the (uncontrollable) model dependence will be weak and it should suffice for models that are not too dissimilar from the HM to use  $H_L^{\text{RFG}}$ . Such a procedure has, for example, been followed in recent experimental re-analyses of the Coulomb sum rule.

The further understanding of the EWSR coming from the model-to-model

comparisons made in the present work also suggest refinements. Specifically, when examining the first moments of the HM and RFG we find that the responses are offset by  $E_S + T_F$ . Shifting the energy transfer by this amount yields the same first moment in the two models. Furthermore, comparing the variances in the two models we find the need for a larger effective Fermi momentum in the RFG to yield agreement with the HM result, which also produces a tendency in the right direction for agreement with experiment. We conclude from these model-to-model comparisons that, with an energy-shift and rescaled Fermi momentum whose origins are now better understood than previously, an effective RFG response can be obtained whose first three energy-weighted moments agree quite well with the HM developed in this work. In the course of reaching this deeper understanding of the two models we have also sharpened our knowledge about the  $y$ -scaling,  $\psi$ -scaling,  $\psi'$ -scaling and Coulomb sum rule properties of quasielastic responses.

## Acknowledgements

It is a pleasure to thank Mrs L. Opisso for the careful typing of the manuscript. The authors also wish to acknowledge the support provided under the M.I.T./I.N.F.N. exchange program during the course of this work.

## References

- [1] A. S. Raskin and T. W. Donnelly. *Ann Phys. (N. Y.)*, 191:78, 1989.
- [2] J. A. Caballero, T. W. Donnelly and G. I. Poulis. *Nucl. Phys.*, A555:709, 1993.
- [3] J. D. Bjorken and S. D. Drell. *Relativistic Quantum Mechanics*. Mc Graw Hill, New York, 1964.
- [4] D. B. Day, J. S. McCarthy, T. W. Donnelly and I. Sick. *Ann. Rev. Nucl. Part. Sci.*, 40:357, 1990.
- [5] T. De Forest, Jr. *Nucl. Phys.*, A392:232, 1983.
- [6] C. Mahaux and R. Sartor. *Phys. Rep.*, 211:53, 1992.
- [7] W. M. Alberico *et al.* *Phys. Rev.*, C38:1801, 1988.
- [8] M. B. Barbaro, A. De Pace, T. W. Donnelly and A. Molinari. *Nucl. Phys.*, A569:701, 1994.
- [9] C. F. Williamson *et al.* (to be published); see also M. S. Osborn, M. S. Thesis, (M.I.T., 1995, unpublished).